DOI: 10.1002/chem.200802424

VIP

Thiophene–Diazine Molecular Semiconductors: Synthesis, Structural, Electrochemical, Optical, and Electronic Structural Properties; Implementation in Organic Field-Effect Transistors

Rocío Ponce Ortiz,[b] Juan Casado,[a] Víctor Hernández,[a] Juan T. López Navarrete,*[a] Joseph A. Letizia,[b] Mark A. Ratner,[b] Antonio Facchetti,*[b] and Tobin J. Marks*[b]

Abstract: The synthesis, structural, electrochemical, optical, and electronic structure properties of a new azine-thiophene semiconductor family are reported and compared to those of analogous oligothiophenes. The new molecules are: 5,5′-bis(6-(thien-2-yl)pyrimid-4-yl)-2,2′-dithiophene (**1**), 5,5′-bis(6-(5-hexylthien-2-yl)pyrimid-4-yl)-2,2′-dithiophene (**3**), and 5,5′-bis(6-(thien-2-yl)pyridazin-3-yl))-2,2′-dithiophene (**2**). Electrochemical experiments demonstrate that introduction of electron-poor heteroaromatic rings into the oligothiophene core significantly enhances electron affinity. Thin-film transistors were fabricated with these materials and evaluated both in vacuum and in air. We find that although diazine substitution is important in tuning oligothiophene orbital energetics, these oligomers are p-channel semiconductors and the field-effect transistor (FET) charge transport properties are remarkably similar to these of unsubstituted oligothiophenes. The combined computational-experimental analysis of the molecular and thin film properties indicates that these diazine-containing oligothiophenes essentially behave as π-extended bithiophenes. Interestingly, despite strong intermolecular interactions, high solid-state fluorescence efficiencies are observed for these new derivatives. Such emission characteristics suggest that these materials behave as more extended π systems, which should be advantageous in light-emitting transistors.

Keywords: density functional calculations · electrochemistry · p-type mobility · semiconductors · transistors

Introduction

Over the past few years, thiophene-based materials have emerged as an important class of semiconductors, embracing chemical structures ranging from small molecules to high molecular weight polymers.[1] The intense research focus these systems have received from the organic materials chemistry community reflects their pronounced chemical/electrochemical stability, the preparative accessibility of many thiophene synthons, and the availability of well-developed/regioselective ring-ring coupling methodologies.[2] Furthermore, the properties of oligo/polythiophene cores can be efficiently tuned by substitution at the terminal core positions as well as by replacing and/or "mixing" some fraction of the thiophene rings with other (hetero)arenes. As a result of these molecularly engineered modifications, a wide variety of electronic and opto-electronic devices having thiophene as the key structural unit have been fabricated.[3] Besides the well-developed field of electrically-conducting solids,[4] these materials are currently under active investigation for applications in organic field-effect transistors (OFETs),[5] light-emitting diodes,[6] lasers,[7] sensors,[8] and photovoltaic cells,[9] as well as for other important technology fields.[10,11,12] For example, an area in which thiophene core substitution has been profitably exploited is in electroluminescent devices, such as lasers and light-emitting transistors,[13] which require electroactive materials also having efficient fluorescent properties.[14] However, unsubstituted/

[a] Prof. J. Casado, Prof. V. Hernández, Prof. J. T. López Navarrete
Department of Physical Chemistry, University of Málaga
Campus de Teatinos s/n, Málaga 29071 (Spain)
Fax: (+34)952-132-000
E-mail: teodomiro@uma.es

[b] Dr. R. P. Ortiz, Dr. J. A. Letizia, M. A. Ratner, Prof. A. Facchetti, Prof. T. J. Marks
Department of Chemistry, Northwestern University
2145 Sheridan Road, Evanston, Illinois 60208-3113 (USA)
Fax: (+1)847-491-2990
E-mail: a-facchetti@northwestern.edu
t-marks@northwestern.edu

Supporting information for this article is available on the WWW under http://dx.doi.org/10.1002/chem.200802424.

alkyl-substituted oligothiophenes generally only exhibit high fluorescence quantum yields in solution.[15] This limitation has been successfully addressed by core-substitution with fluorescence-enhancing groups such as phenylene,[16] biphenylene,[17] fluorene,[18] bis(methylphenyl)aminophenylene,[19] and bis(9,9-dimethylfluorenyl)aminophenylene.[20]

Organic FETs represent another important area in which oligo/polythiophenes have been successful,[5] starting from the pioneering work of Hotta, Garnier, and Katz on oligothiophenes,[21] and Tsumara and Assadi on polythiophenes.[22] Since these initial studies demonstrating p-channel FET operation, much effort has focused on tuning key oligo/polythiophene FET properties to optimize carrier mobility, air-stability, and to enable electron- (n-channel) and ambipolar transport.[23] These efforts have included the synthesis of variously functionalized oligo/polythiophene derivatives, optimization of film growth processes by means of specific solvents, and fabrication of device structures and/or pairing with semiconductor properties-enhancing gate dielectrics.[24] From a chemical perspective, molecular structure modifications offer the promise of new properties and functions. For example, n-channel semiconductors for OFETs are rare, and even rarer are those containing ostensibly electron-rich thiophenes. Although the design rules for n-channel organic semiconductors are in some ways similar to those for the corresponding p-channel materials, with the exception that efficient injection of electrons into the LUMO must occur, the actual realization of new, stable n-channel materials remains a daunting challenge. For example, n-channel oligothiophenes were realized by a number of us, beginning in 2000, by introducing fluorocarbon substituents.[5b,c] However, from an electronic structure/redox properties viewpoint, n-channel fluorocarbon-substituted oligothiophenes, especially those having large π-electron cores, exhibit relatively modest properties variations compared to the corresponding p-channel alkyl-substituted parent systems. Therefore, the origin of the remarkable FET majority carrier sign inversion upon fluorocarbon substituent introduction and whether this inversion principally reflects enhanced core electron affinity, and whether other important factors are operative, remains unresolved.

Nitrogen-containing, electron-poor heterocycles have previously been incorporated in, and combined with, thiophene-based conjugated structures to achieve donor-acceptor copolymers with reduced band-gaps.[25,26,27] In this regard, azines have attracted recent attention, owing to their biological properties,[28] their potential applicability in bond-formation processes,[29] in liquid crystal design,[30] as well as in non-linear optical materials.[31] However, there are very few examples of azine materials in the organic electronics area and even fewer based on oligomeric structures. For example, Katz first reported on the FET properties of thiophene-thiazole derivatives exhibiting p-channel activity and very large I_{on}:I_{off} ratios,[32] whereas more recently, Jenekhe and Yamamoto reported promising thienopyrazine-, quinoxaline-, and thienodithiazole-thiophene co-polymers, again exhibiting p-channel transport.[33] These interesting results raise the question of how key molecular/charge transport properties might respond to introducing even more strongly electron-accepting heterocycles into such structures. Here we report the synthesis of a new series of mixed diazine-thiophene oligomers **1**–**3** (Figure 1), in which the diazine is a pyridazine or pyrimidine unit, and compare and contrast their properties with those of the unsubstituted oligothiophene cores **4**–**6**. These nitrogen-containing heterocycles were selected because of their more positive reduction potentials and greater electron-withdrawing capacities than other monocyclic pyridines and thiazoles,[34] the ready access to key synthetic building blocks, and the current general research goals in organic electronics of: 1) Discovering new high-mobility organic semiconductors, optimally solution-processable; 2) enabling new n-channel materials and functions; 3) stabilizing n- and p-channel operation in ambient.

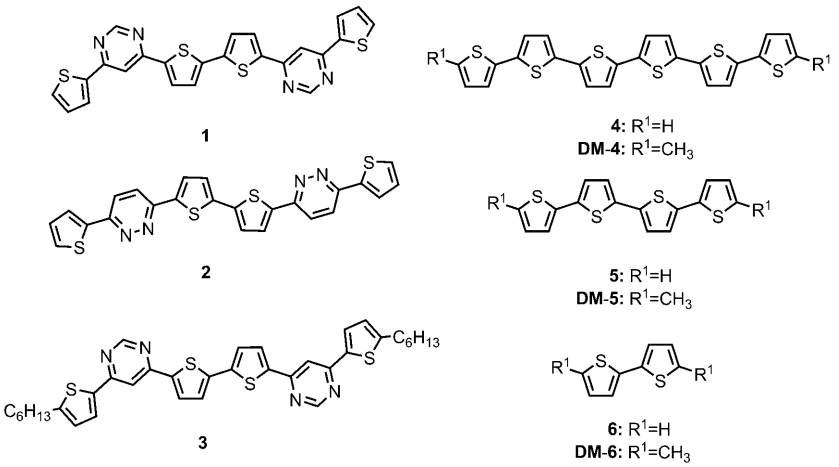

Figure 1. Chemical structures of the diazine-thiophene and thiophene oligomers examined in this study.

We show here that the new azine-based targets can be efficiently synthesized in good yields and characterize them by a combination of thermal (thermogravimetric analysis and differential scanning calorimetry), optical spectroscopic (UV/Vis, photoluminescence, and Raman), and electrochemical (cyclic voltammetry) techniques. DFT computations provide valuable insights into key molecular electronic structure and thin film properties. In addition, vapor-deposited films of these new molecules are investigated by X-ray diffraction (XRD) and scanning electron microscopy (SEM). Finally, thin-film transistors are fabricated and eval-

uated both in vacuum and in air. Our results demonstrate that oligothiophene molecular electronic structure and FET majority charge transport properties respond in very different, and not necessarily intuitive, ways to diazine skeletal introduction.

Results and Discussion

Synthetic strategies: The new azine-thiophene oligomers **1**, **2**, and **3** were synthesized according to Scheme 1. The starting materials for oligomer realization are readily available,

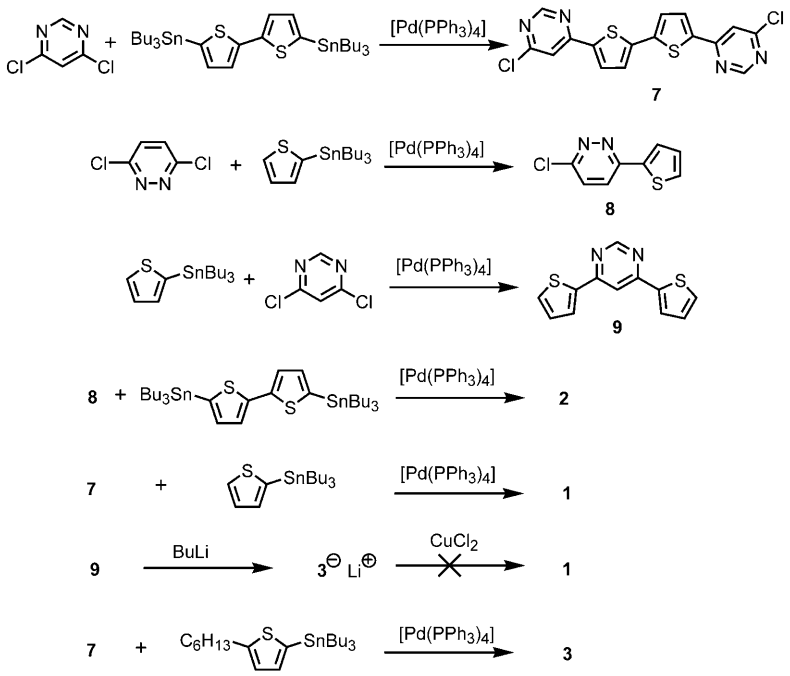

Scheme 1. Synthetic Scheme for the new azine-thiophene oligomers.

and the general synthetic strategy entails α,ω-distannylation of thiophene and dithiophene, followed by Pd-catalyzed Stille coupling with the appropriate azine building blocks. Key pyrimidine intermediate **7** was synthesized in ≈70% yield by $[Pd(PPh_3)_4]$-catalyzed cross-coupling of 4,6-dichloropyrimidine with 5,5′-bis(tri-*n*-butylstannyl)-2,2′-dithiophene in toluene. The final two pyrimidine-thiophene oligomers, **1** and **3**, were accessed by means of the coupling of core **7** with 2-(tri-*n*-butylstannyl)-thiophene and 2-(tri-*n*-butylstannyl)-5-hexylthiophene, respectively. Compounds **1** and **3** were obtained in ≈50 and 70% yields, respectively. Note that because of the relatively low yields, we attempted to synthesize **1** through $CuCl_2$-promoted dimerization of the lithium salt of **9**, however this was unsuccessful.

Pyridazine-thiophene building block **8** was obtained in ≈50% yield by coupling of 3,6-dichloropyridazine with 2-(tri-*n*-butylstannyl)-thiophene. Compound **2** was subsequently synthesized by coupling compound **8** with 5,5′-bis(tri-*n*-butylstannyl)-2,2′-dithiophene (≈86% yield). Compounds **1** and **2** were purified by gradient vacuum sublimation, whereas more soluble **3** was purified by recrystallization.

Molecular structure-property relationships

Thermal characterization: Differential scanning calorimetry (DSC) was performed on all the new thiophene-diazine materials and reveals that the entire set is thermally stable, with DSC plots showing no evidence of mesophase formation before melting (Figure S1). This is surprising considering the rod-like molecular structures and the established presence of multiple LC transitions in thiophene homo-oligomers and phenylene-thiophene co-oligomers.[35] Thermogravimetric analysis (TGA) reveals quantitative sublimation in all cases (Figure S2), demonstrating the thermal robustness of the **2** and **1** cores. Note that this result stands in contrast to some alkyl-substituted and longer unsubstituted oligothiophenes,[36] and despite the very high melting points (see the Experimental Section), oligomers **1**–**3** sublime quantitatively without significant decomposition. Intra- and inter-molecular nonbonded contacts, discussed in next sections, may also contribute to this effect.

Electrochemistry: The electrochemistry of oligo- and polythiophenes reveals important aspects of chemical/electronic structure, charge injection and storage mechanisms, substituent effects, and other physical characteristics.[36,37,38] Such studies have aided thiophene-based conductor development, quantitatively addressing substituent oligomer dimension effects. Cyclic voltammetry (CV) for oligomers **1**–**6** was performed under N_2 in 0.1 M THF/$TBAPF_6$ solutions with scanning rates between 60–150 $mV\,s^{-1}$. Most systems exhibit one or two reversible and/or quasi-reversible one-electron oxidation and reduction waves within the solvent/electrolyte window range. Figure 2 shows representative voltammograms whereas the electrochemical data are summarized in Table 1 below. When the voltammograms are (quasi)reversible, it is possible to extract formal potentials ($E^{1/2}$), as the midpoints between peak potentials for the forward and reverse scans. Unsubstituted oligothiophenes, with the exception of **6**, exhibit two reversible reduction potentials, whereas reversible oxidations are observed only for **4**.[38,39,40] Two single-electron reductions (versus SCE) are observed at −1.45/−1.57 V for **1**, at −1.45/−1.56 V for **3**, and at −1.48/−1.64 V for **2** versus −1.71/−1.86 V for **4**. Irreversible oxida-

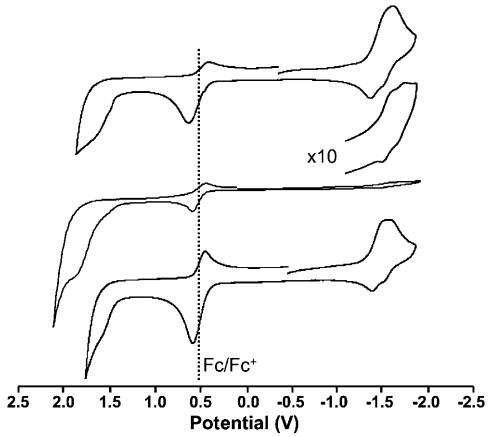

Figure 2. Cyclic voltammograms (first scan, $v = 80\,\mathrm{mV\,s^{-1}}$) in THF on a 0.8 mm diameter glassy carbon electrode for thiophene-diazines **1** (top), **2** (middle), and **3** (bottom).

Table 1. Anodic (E_a), cathodic (E_c), and half ($E^{1/2}$) potentials [V] versus SCE of compounds **1–6** in dry THF under nitrogen.[a]

Compound	Oxidation						Reduction					
	Anodic		Cathodic		Half		Cathodic		Anodic		Half	
	E_{a1}	E_{a2}	E_{c1}	E_{c2}	$E_1^{1/2}$	$E_2^{1/2}$	E_{c1}	E_{c2}	E_{a1}	E_{a2}	$E_1^{1/2}$	$E_2^{1/2}$
1	1.63						−1.51	−1.63	−1.39	−1.51	−1.45	−1.57
2	1.87						−1.52	−1.66	−1.44	−1.61	−1.48	−1.64
3	1.60						−1.50	−1.60	−1.40	−1.52	−1.45	−1.56
4	1.02	1.17	0.93	1.08	0.98	1.13	−1.76	−1.91	−1.66	−1.79	−1.71	−1.86
5	1.40		0.81	1.00	1.10		−2.02	−2.33	−1.86	−2.20	−1.94	−2.07
6			0.77	1.12			−2.60		−2.24		−2.42	

[a] Referenced to the Fc/Fc^+ couple in THF (0.50 V vs. Ag/AgCl; 0.54 V vs. SCE).

tive features are observed at ≈+1.6 V for both pyrimidine-based systems and at ≈+1.87 V for **2**, versus reversible oxidations at +0.98/+1.13 V for **4**. This solution phase redox behavior contrasts with the results of thin-film transport measurements for which it will be seen that electrons are far less mobile than holes (vide infra), confirming the observation that OFET charge transport is often dominated by charge trapping at the semiconductor-dielectric interface rather than by intrinsic molecular redox properties.[41] There are, however, other factors that likely influence transport properties from the perspective of molecular charging such as internal molecular reorganization energies for cation or anion generation, that will be discussed in the closing section in connection with OFET carrier mobility.

Analysis of the thiophene-diazine half-wave potentials reveals interesting trends. Compared to π-isoelectronic **4** having the same number of π electrons with the N and S atoms included, the reduction potentials $E_1^{1/2}$ and $E_2^{1/2}$ of **1–3** are shifted towards substantially more positive values [$\Delta E_1^{1/2}$ (**4**→**1–3**) = +(0.23-0.26) V, $\Delta E_2^{1/2}$ (**4**→**1–3**) = + (0.22–0.30) V] in agreement with the very electron-deficient nature of azines compared to thiophenes. Furthermore, within the diazine-thiophene family, the reduction potentials are shifted to more negative values on proceeding from pyrimidine to pyrazine systems [$\Delta E_1^{1/2}$ (**1**, **3**→**2**) = −(0.03) V, $\Delta E_2^{1/2}$ (**1**, **3**→**2**) = −(0.08) V], corroborating the greater charge demands (defined as the capacity of the heterocycle to stabilize additional negative π charge)[42] of the former heterocycle. In marked contrast, for alkyl-/fluorocarbon-substituted oligothiophenes, the electrochemical potential difference between subsequent reduction events [$\Delta E^{1/2} = |E_2^{1/2} - E_1^{1/2}|$] does not track the increased stabilization of the negative charge. For equivalent π-delocalized systems, the compression of $\Delta E^{1/2}$ indicates a reduction of Coulombic repulsion between excess negative charges. Hence, the value in **4** (0.15 V) is similar to that in **2** (0.16 V), likely reflecting the identical *para*-connection of cores having the same number of π electrons. The $\Delta E^{1/2}$ value is similar in **1** (0.12 V), however, the $\Delta E^{1/2}$ differences among these three molecules are too small to clearly ascribe to a particular electronic or structural characteristic. Moreover, when doubly charged species are involved, Coulombic repulsions can play a significant role.[43]

Regarding anodic processes, the same enhanced electron demand argument or inclusion of more electronegative N atoms can be invoked to explain the oxidative events occurring at more positive potentials.

Optical Properties: Optical absorption and fluorescence emission spectra of compounds **1–6** were measured in both solution and as powders/vapor-deposited thin films (Figure 3) to assess the effect of azine substitution on oligothiophene absorption/emission maxima ($\lambda_{abs}/\lambda_{em}$) and the (optical) HOMO–LUMO energy gap. Table 2 collects UV/Vis-PL data for all compounds in THF solution. The solution absorption spectra of **1–3** exhibit incipient vibronic fingerprints, clearly distinguishable at lower temperatures (see Figure S3 in the Supporting Information), whereas in the fluorescence spectra, typical subpeaks are observed even at room temperature (Figure 3). This finding likely reflects full core planarization upon electron excitation and relaxation to an S_1 qui-

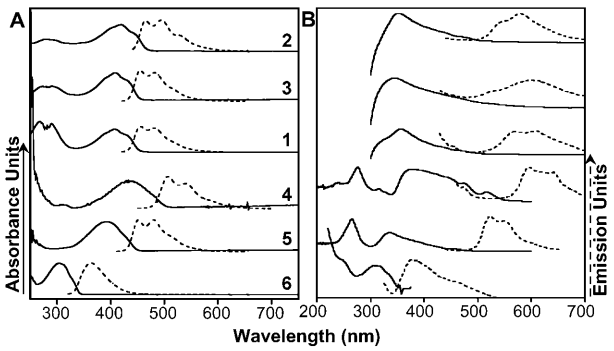

Figure 3. Optical absorption (solid lines) and emission (dashed lines) spectra of compounds **1–6** in A) THF and B) the solid state.

Table 2. Optical absorption (maximum of absorption, λ_{max} and extinction coefficient at λ_{abs}, ε) and emission (maximum of fluorescence, λ_{em} and quantum yield, Φ_f) data[a] for compounds **1–6** in dry THF and in the solid state (50 nm films).

Compound	Solution					Film			
	λ_{max} [nm]	ε [$M^{-1}cm^{-1}$]	λ_f [nm][a]	Δ[b] [eV]	Φ_f[c]	λ_{max} [nm][a]	λ_f [nm][a]	Δ[b] [eV]	E_g^{op} [eV]
1	408	72700	455	0.31	0.38	350	610	–	2.4
2	420	40100	465	0.29	0.24	344	590	–	2.2
3	409	65500	455	0.31	0.42	356	605	–	2.7
4	436	50000[a]	505*, 539	0.39	0.46	376	589	1.19	2.3
5	391	35000	450*, 478	0.42	0.20	336	520	1.31	2.7
6	304	12800	363	0.66	0.01	–	–	–	–

[a] Absolute maximum indicated by asterisk, [b] $\Delta=\lambda_{em}-\lambda_{abs}$, [c] Measured using quinine sulfate as the standard.

noidal emissive state. As will be discussed below, conformational freedom (rotation about inter-ring C–C single bonds) in the solution ground electronic state of the azine-containing molecules is more restricted than in π-isoelectronic **4** in which the solution ground state is, on average, more twisted. The splitting periodicity of the vibronic peaks in absorption is estimated to be ≈1400–1500 cm^{-1}, and can be assigned to collective, totally symmetric oligothiophene core ν(C=C) stretching modes, vibronically coupled to the electronic excitation and hence resonance-enhanced in the Raman spectra (see below). As will be discussed below, this result establishes a connection between molecular electronic and vibrational properties.

The large molar absorption coefficients (ε, Table 2) indicate dominance in the optical spectra of allowed, conjugated core π→π* transitions. As expected, λ_{max} values increase across the series for increasing numbers of ring units (**6**→**5**→**1**–**4**). Within the π-isoelectronic systems **1**–**4**, λ_{abs} increases on proceeding from **1** (408 nm) to **2** (420 nm) to **4** (436 nm). Although the shorter wavelength absorption of **1** might be explained by reduced π-conjugation, owing to the azine-thiophene meta linkage, the result for **2** is surprising since mixing electron-rich and electron-poor rings is a proven strategy for achieving small-bandgap chromophores.[44] Analysis of the orbital composition of the HOMO→LUMO excitation rationalizes these observations (vide infra). In contrast to **4**, the HOMO of the isoelectronic nitrogen-containing molecules is localized mainly on the central bithienyl unit, whereas the LUMO is heavily centered on the vicinal pyrazine or pyrimidine rings. However, in **4** the HOMO/LUMO topologies involve the entire thiophene core, rendering electronic repulsion accompanying the excitation less pronounced than in **1**–**3**. Thus, the **1**–**3** vs. **4** λ_{max} differences not only reflect the intrinsic HOMO–LUMO gaps but also the nature of the optical excitation. That is, the HOMO–LUMO excitation in **1**–**3** represents an expansion of electron density (localized in the **6** portion for the HOMO, delocalized over the entire conjugation pathway for the LUMO), in contrast to the case in homogeneous oligothiophenes **4**–**6**.

Fluorescence emission spectra of compounds **1**–**6** were measured in THF by exciting 10^{-5}–10^{-6} M solutions at the corresponding λ_{max} values. The shapes of the fluorescence excitation spectra track those of the absorption spectra. Photoluminescence quantum yields (Φ_f) were determined using a quinine sulfate standard,[45] and PL data are also collected in Table 2. Intrinsically, Φ_f is determined by the relative rates of nonradiative and radiative deactivation. For the present series, Φ_f values in **1**–**6** are found to increase quasi-monotonically with the number of rings. This behavior is reminiscent of that found in the α-**4**–**6** series, in which Φ_f increases in molecules having up to 6 rings and then remains constant or even decreases for longer oligomers.[46] Fluorescence quantum yields are found to increase on proceeding from **6** to **4** and then to decrease in the thiophene-azine systems. The azine-centered HOMO–LUMO optical transition, with the HOMO localized principally on the central bithienyl unit, occurs at shorter wavelengths than that of **4**. This corresponds to an enlargement of the optical gap or decreased π-conjugation relative to **4**. Consequently, a slight reduction in Φ_f is not unexpected on going from **4** to the azine derivatives. This property is therefore midway between those of **6** and **4**. Note that owing to the dominant role of the large sulfur orbital angular momentum in **6**, efficient intersystem crossing strongly decreases the fluorescence yield of this short oligomer.[47]

The changes in thiophene-diazine conformations to more planar structures and energy dissipation within the excited state lifetime is manifested in marked Stokes shifts, the energy differences between the 0–0 transitions in absorption and emission.[48] Since 0–0 transitions are rarely observed in room temperature solution spectra, it is accepted procedure to use $\Delta=\lambda_{em}-\lambda_{abs}$ to index the magnitude of the Stokes shift. The observed general trend here is that Δ decreases with increasing numbers of heterocyclic rings, and furthermore, when thiophene is replaced by an azine moiety. The amplitude of this shift generally tracks the lifetime and structural reorganization of the excited state,[48] with longer lifetimes corresponding to increased relative probability of non-radiative decay and correlating with lower PL quantum efficiency. Indeed, these trends are in good agreement with the present quantitative Φ_f measurements.

Solution optical gaps (E_g^{op}), defined by the 0–0 transition energies, were estimated from the intercept of the normalized optical absorption and emission spectra, regarded as the mirror of the 0–0 transitions.[49] Within the thiophene series, the gaps decrease with extension of the core structure, from 3.75 eV (**6**) to 2.89 eV (**5**) to 2.61 eV (**4**) (Table 2). In contrast, when one of the thiophene units is replaced by a diazine ring, E_g^{op} values increase to 2.95–3.04 eV, much larger than those of **5** and **4**, and comparable to those of short phenylene-thiophene oligomers.[50] The present re-

sults for E_g^{op} are expectedly similar to those for λ_{abs}, however the Δ data may indicate that structural changes (i.e., planarization) after excitation are smaller in the azine derivatives, an effect in agreement with greater planarization in the solution ground electronic state as a consequence of thiophene-azine through-space intramolecular interactions, as discussed below.

Solid-state optical absorption/PL data for molecules **1**–**5** are collected in Table 2. The film absorption spectra exhibit characteristic transitions at high energy (270–280 nm) found in the spectra of all oligothiophenes and originating in the thiophene ring.[51] The position and shape of the high energy $\pi\rightarrow\pi^*$ transitions reflect the interplay of molecular structure, core length, and solid state packing. In general, a bathochromic shift of this absorption is observed as the core length increases on going from **5** to **1**–**4**. Compared to solution values, the maxima of the strongest π–π^* absorptions are shifted to shorter wavelengths in the thin film spectra, as a result of excitonic interactions between closed-packed nearest-neighbor molecules. The coupling between the transition dipoles of molecules at crystallographically nonequivalent sites leads, in the case of a rigid infinite lattice, to well-known Davydov splitting.[52] When the dipoles are all parallel, the transition between the ground state and the lower crystal excited state is strictly forbidden, thus accounting for the unique intense peak. In analogy to previous oligothiophene results,[53] the weak unresolved absorption at longest wavelengths–a low energy tail of the intense band ($\approx$450 nm) in solid compounds **1**–**3** can be attributed to the 0–0 transition of isolated molecules, either located in disordered domains or at grain boundaries, where molecular misalignment can lead to weak intermolecular coupling and minimal splitting of the excited levels. In fact, the absorption tails of the intense absorptions closely parallel the trends observed in solution. The shoulders on the highest energy side of the intense solid state absorptions may result from the corresponding C=C vibronic replica.[51]

Film photoluminescence spectra were obtained by λ_{max} excitation, and data are compiled in Table 2. The spectral shapes and maxima strongly depend on molecular structure, with most plots exhibiting additional peaks/shoulders. The spacings between the better-resolved peaks (1300–1500 cm^{-1}) suggest coupling with excited state vibrational modes, probably thiophene C=C stretches along the quinoidal molecular backbone. Extraction of film E_g^{op} parameters is less straightforward, owing to the multiple absorption/emission transitions. However, reasonable estimates of E_g^{op} values can be obtained from the onset of the absorption (at 10% of the maximum). Similar to the solution trends, E_g^{op} values decrease as the core conjugation length increases and are larger for the azine-substituted systems. In general, film E_g^{op} values are smaller than the corresponding solution values by 0.1–0.4 eV. A similar trend is observed for oligothiophenes.[54]

Molecular structural features from vibrational spectra: Figure 4 shows Raman spectra of the present thiophene-azine compounds along with those of the α,ω-dimethyl-substituted oligothiophenes; **DM-6**: α,ω-dimethylbithiophene, **DM-5**: α,ω-dimethylquaterthiophene, **DM-4**: α,ω-dimethyl sexithiophene. **DM-6** was selected to compare its electronic structure to that of the **6** central unit of **1**–**3**. We first consider the most intense Raman bands (Figure 4) originating from the C=C stretching modes of the central bithienyl fragment. This transition is an important molecular structure fingerprint. The degree of bond length alternation (BLA), estimated as the average sum of the distance differences between successive C=C/C−C bond pairs of each thiophene ring is related to the ring C=C stretching mode associated with the strongest Raman line.[55] This Raman transition varies from 1498 to 1477 cm^{-1}, on going from **DM-6** to **DM-4**, whereas in the isoelectronic diazine compounds the analogous feature is located at 1481 cm^{-1} in **1** and 1470 cm^{-1} in **2**. This fall in frequency (relative to **DM-6**) is in agreement with the pronounced reduction of the bithiophene B3LYP/6-31G*-computed BLA values, which vary from 0.051 Å for **DM-6** to 0.028 Å for **1**, and 0.031 Å for **2**. Note that similar Raman frequency downshifts are observed for lines primarily associated with the C=C stretching mode located at $\approx$1550 cm^{-1}.

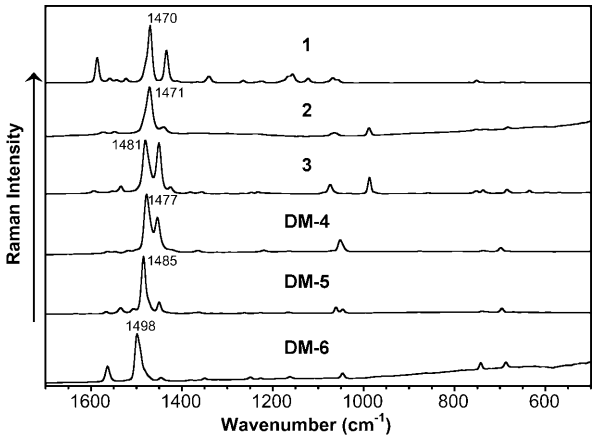

Figure 4. Powder FT-Raman spectra (λ = 1064 nm excitation) of thiophene-diazines, **1**–**3**, and unsubstituted oligothiophene compounds, **4**–**6**.

Particularly significant also are the discrepancies between the Raman line positions in **1** (1481 cm^{-1}) and **2** (1470 cm^{-1}), and the opposite behavior of the corresponding computed BLAs (0.028 and 0.031 Å, respectively). The assignment of *ring* BLAs is based on the *ring* character of the stretching vibrations. However, as will be shown later, intramolecular S···N interactions favor polyene-like inter-ring conjugation which should be evaluated not only as intra-ring distances but also as CC bonds connecting both internal thiophenes (note that the intra-ring C=C/C−C modes will be strongly coupled to C−C inter-ring stretching transitions). These distances decrease somewhat on proceeding from **1** and **3** to **2**, supporting the evolution of π–conjugation in accord with the aforementioned falling energy gaps and the concurrent downshifting of the most intense Raman bands. Analyzing these effects further, Figure 5 shows the FT-

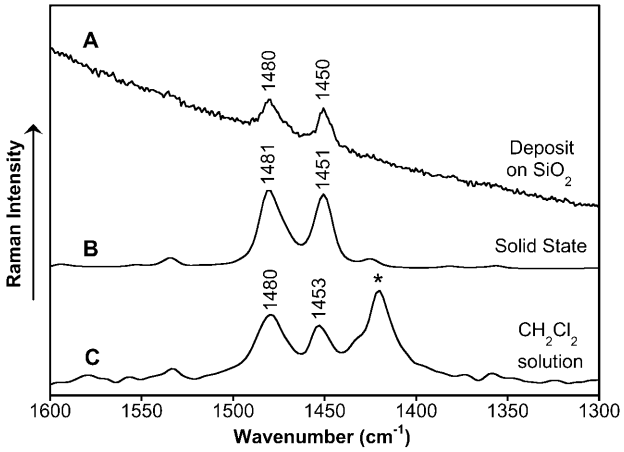

Figure 5. $\lambda = 1064$ nm FT-Raman spectra of **1** in A,B) the solid state and C) in a CH_2Cl_2 solution. The Raman spectra of the solid samples were taken with a $\lambda = 514.4$ nm laser excitation. The band with an asterisk denotes a solvent vibration.

Raman spectra of **1** as a powder and as a thin film deposited on a Si/SiO_2 substrate (likely containing both amorphous and crystalline forms, see below) as well as in the solution phase. In all cases, the energies of the most intense Raman transitions are very similar, indicating a strong tendency for **1** to planarize, even in solution. Because of the lack of strong intermolecular interactions in solution, this observation corroborates the existence of substantial intramolecular S···N attractions favoring planar conformations.[56] The present hypothesis concerning weak S···N interactions in thiophene-azine derivatives is supported by literature crystallographic data on similar thiophene-azine molecules (Figure 6; see Figure 8 below for a sketch), which indicate short solid state S···N distances, similar to those argued here for **1**, **3**, and **2**.[57] Such interactions are also evident in the computational results discussed below for our compounds. The accuracy of theoretical molecular geometries can be tested in one of the reference systems in Figure 6, for instance the experimental S····N distance of 2.93 Å is theoretically reproduced as 2.95 Å at the B3LYP/6-31G** level.

Electronic structure computation: Theoretical modeling of thiophene-diazine electronic structures was performed in parallel with the present experimental work. The parent oligothiophenes were previously studied as polythiophene models and as important representative π-electron organic materials.[58] The utility of such modeling has advanced with increased reliability of DFT methods, which now provide accurate estimates of molecular geometries,[59] including dihedral angles and rotational barriers,[60] dipole moments,[61] as well as electronic structure properties such as electron affinity,[62,63] ionization potential,[64] band gaps and ground state vibrational frequencies.[65,66] To ensure the most meaningful comparison, the entire **1–6** series was analyzed using the same computational methodology (see the Computational methods for details).

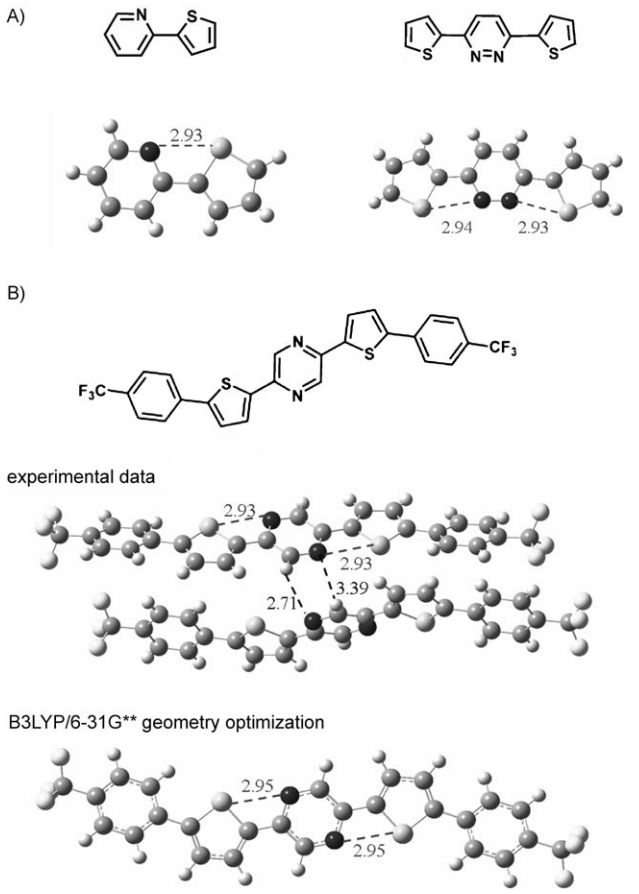

Figure 6. A) X ray crystal structures of molecules similar to the present thiophene-azines exhibiting short intra(inter)molecular S···N contacts (distances are in Å).[57a,c,d] B) Theoretical geometry for one representative case is also shown.

The optimized geometries of molecules **1–6** provide metrical parameters for comparison with the experimental dimensions from single-crystal X-ray diffraction.[67] Table 3 summarizes molecular core lengths (maximum ring carbon-ring carbon distance along the axis of the oligothiophene core) and maximum lengths (the greatest extent of the molecule, including the side-chains) illustrating, for the oligothiophenes, the excellent agreement between computed molecular geometries and experimental crystal structures.[68] The lengths of the oligothiophene cores are very similar for various ring substitutions, indicating that the rigidity of the conjugated cores parallels the long molecular axes, with the common all-*anti* heterocycle conformation prevalent in all oligomers. Each additional thiophene unit is computed to increase the length of the core by 3.91 Å on average (vs. 3.87 Å from experiment).[68] Similar effects are also observed in computed dipole moment trends for the series **1–6** (Table 3). These largely symmetric molecules have modest dipole moments.[69]

Important information on HOMO and LUMO energies derives from analysis of the experimental electrochemical and optical data, supplemented by theoretical calculations. Table 4 summarizes electrochemical, optical, and computed

Table 3. Computed metrical parameters for molecules **1–6** derived from DFT//B3LYP/6-31G** optimized coordinates.

Compound	Length [a,b]		Avg. Dihedral	μ [D]
	Core [Å]	Maximum [Å]	Angle [°][b]	
1	9.83	25.87	0	0
2	9.83	26.75	0	0
3	9.83	38.82	0	0.584
4	25.51 (25.29, 25.31)	26.59 (26.14)	0.5 (0.5, 0.8)	0.023
5	17.67 (17.55, 17.48)	18.75 (18.17)	0.5	0.020
6	9.83 (9.76, 9.72)	10.90 (10.61, 10.90)	1.7 (0.0)	0.022

[a] Core length refers to the maximum distance from ring carbon to ring carbon atom along the thiophene long axis excluding the lateral hexyl groups in **3**, whereas the maximum length is the greatest extent of the molecule, including side chains. Both lengths include standard van der Waals radii for carbon (1.70 Å), and hydrogen atoms (1.20 Å). [b] Numbers in parentheses indicate experimental values from X-ray crystal structures (see Ref. [67]).

Table 4. Comparison of electrochemical, optical, and computed HOMO–LUMO energy gap (E_g) and absolute HOMO and LUMO energies for molecules **1–6**.

Compound	E [eV]				E_g [eV]		
	Experimental[a]		Theoretical				
	HOMO	LUMO	HOMO	LUMO	E_g^{CV}[b]	E_g^{op}[c]	E_g^{th}[d]
1	−6.64	−3.39	−5.62	−2.45	3.05	3.04	3.17
2	−6.64	−3.36	−5.26	−2.32	3.28	2.95	2.94
3	−6.47	−3.39	−5.52	−2.35	3.08	3.04	3.17
4	−5.82	−3.13	−4.79	−2.18	2.69	2.61	2.61
5	(−5.79)	−2.90	−4.95	−1.93		2.89	3.02
6	(−6.22)	−2.42	−5.47	−1.25		3.75	4.22

[a] LUMO energy estimated from the relationship: LUMO (eV) = $-4.84\,\text{eV} - e\,E_{1/2,\text{Red}}$. HOMO energy estimated from the relationship: HOMO (eV) = LUMO $- E_g^{CV}$. The values reported in parenthesis are estimated using the optical gap. [b] From electrochemical data: $E_g^{CV} = E^{1/2}_{1,\text{Ox}} - E^{1/2}_{1,\text{Red}}$. [c] From optical spectroscopic data. [d] From DFT computation.

energy gaps (see Figure 7) for compounds **1**,**2** and **4–6**. The first important observation is the excellent agreement between solution E_g^{CV} and E_g^{op} data, with differences of only ≈0.1–0.2 eV for almost all molecules. Since these are two independently derived measurements, the good agreement supports the accuracy of the results. Table 4 also summarizes the experimental and computed LUMO and HOMO energies, calculated from the first reduction potentials ($E_1^{1/2}$) and from the onset of oxidation, respectively.[70] Although HOMO and LUMO eigenvalues from DFT methods cannot be formally taken as either rigorous ionization potentials or electron affinities,[71] previous work has shown that B3LYP-derived eigenvalues compare favorably with experimental ionization potentials and slightly less well with electron affinities.[62,63] The principal disparity between computed and electrochemical HOMO/LUMO values doubtless reflects the differences in environments (solvation), and previous work has shown that parameters such as polarizability and cavity radius can be used to linearly adjust (by means of a Kamlet–Taft relationship)[72] computed ionization potentials and electron affinities for solvation to allow comparisons with electrochemical data.[73]

Finally, the energy gaps also demonstrate excellent overall agreement between electrochemical and optical data and the computed DFT orbital energies, although the theoretical gaps predicted from vertical transitions are somewhat greater in energy than the E_g^{CV} or E_g^{op} data in Table 4, as expected. Assuming the validity of the Koopmans approach, the slight increase in the reduction potential for **2** relative to **1** is consistent with the LUMO destabilization observed in Figure 7. In the case of **2** (with two vicinal N atoms) only one of the two N atoms participates in the LUMO, whereas in **1**, both heteroatoms contribute at the expense of one vicinal carbon. The greater electronegativity of N vs. C depresses the LUMO and renders reduction more favorable. From the CV experiments (Table 1) it is found that **2** and **1** oxidation processes occur at more positive potentials (0.2–0.6 V) than in **5** and **4**, where electrochemical generation of the

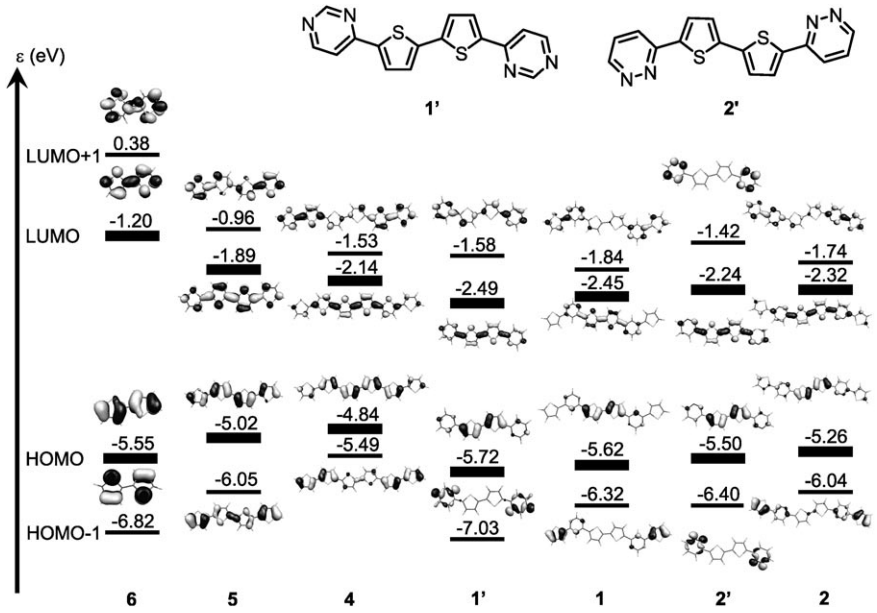

Figure 7. DFT//B3LYP/6-31G** derived topologies and energies of the indicated frontier MOs for molecules **1–6**.

corresponding cationic species is observed at 1.1–1.13 V. Indeed, the thiophene-azine redox parameters are energetically similar to those of **6**. This can be rationalized by considering: i) computed thiophene-azine HOMO levels are rather close in energy to those of bithiophene (see Figure 7). This similarity is accentuated in the pyrimidyl derivative owing to cross-conjugation: ii) The HOMO wavefunctions are primarily centered on the bithienyl fragment: iii) Although thiophene-azine derivative π-conjugation is greater than in **6**, the aforementioned S···N interactions will moderate the thienyl sulfur (which becomes more electropositive) electron donor capacity. In this regard, it appears that electron wavefunction extension and S···N coupling effects largely cancel each other.

The thiophene-azine derivatives all exhibit a strong solid state optical absorption band at 410-420 nm (see Figure 3) with characteristic vibronic components on both sides of the maximum. According to the present time-dependent (TD)-DFT calculations, these intense bands correspond to one-electron HOMO→LUMO excitations. For **1**, the absorption maximum is computed at 433 nm with an oscillator strength of $f=1.62$, which is by far the most intense of all the excitations. In contrast to **6**, the observation of vibronic replicas in these mixed co-oligomers can be explained by the nature of the azine N-electron lone pairs which can engage in hydrogen-bonding with neighboring molecules (see Figure S4 in the Supporting Information), thus conferring extra rigidity on the molecular skeleton and, as a result, the observed vibronic structure. On the other hand, this type of interaction may favor head-to-tail or lateral intermolecular interactions instead of co-facial π-stacking, which may be unfavorable for charge transport. For the same reasons, one expects non-negligible intramolecular S···N interactions. Two facts support this: i) The sum of the S and N atomic radii is 3.350 Å, although the present calculations estimate these distances to be significantly shorter, 2.922 Å in **1**, and 2.916 Å in **2** (Figure 7,8); and ii) the optimized geometry of **2** predicts the C=C bonds of the pyridazyl and thiophene connected groups (i.e., Kekule resonance structures) to be in a *syn* conformation. It is well established that, in the absence of additional effects, the *trans* isomers are generally more stable.[74] Figure 8 also shows the computed B3LYP/6-31G** rotational barriers about the thiophene-pyrimidine (TPm) and thiophene-pyridazine (TPr) bonds (i.e., as models of **1** and **2**) which reveal that the *syn* (i.e., 180°) conformation is the most stable. The rotational barrier for **6** is also shown for comparative purposes. From Figure 8, note that the rotation barriers for the *syn-anti* interconversion are larger in the diazine oligomers than in **6**, in agreement with the greater rigidity, owing to the through-space S···N interactions. Furthermore, these interactions are also responsible for stabilizing the *syn* isomer in the diazine-thiophene derivatives, whereas the *anti* disposition is invariably preferred in unsubstituted oligothiophenes.

At the intramolecular level, substitution of **6** with two pyrimidyl groups (see Figure 7) slightly stabilizes the HOMO, likely owing to inductive effects (note that there is minimal

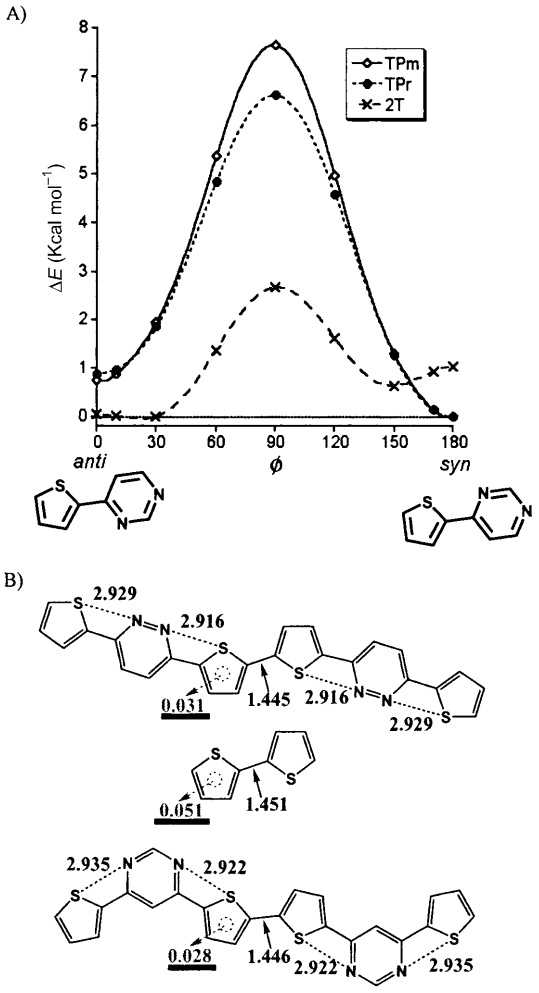

Figure 8. A) B3LYP/6-31G** computed rotational barriers for TPm and TPr as models of **1** and **2**. Molecule **6** is also shown for comparison. B) Theoretical predicted distances in Å;. Ring BLAs are shown underlined (Å).

π-interaction between the aromatic thiophenes and the pyrimidyl groups). This observation is based on the cross-conjugated character of the pyrimidyl groups relative to bithiophene for this orbital. For the pyridazyl analogue, the interaction with the bithiophene core leads to linear π-conjugation, and results in the highest HOMO energy within the series. In contrast, the LUMO wavefunction displays a bonding interaction between the thienyl core and the pyrimidyl moieties, leading to an effective inter-ring C=C/C–C conjugation in the central bithiophene which extends towards the outermost groups. As a result, the LUMO energy is more stabilized than its HOMO counterpart. Further substitution of the above molecular fragments with two external thiophene rings does not alter the HOMO/LUMO wavefunctions, causing only slight modifications of the energies. As a whole, the **6**→**1** transition results in a net reduction of the HOMO/LUMO gap in agreement with the observed reduction of the optical gap associated with the HOMO–LUMO photoexcitation and E_g^{op}. The **1**→**2** progression

causes an additional narrowing of the HOMO–LUMO energy gap, owing to simultaneous HOMO and LUMO destabilization, more pronounced for the former MO. The greater destabilization of the HOMO on going from **1**→**2** can be rationalized as follows: i) Inductive effects are partially removed as a result of the N–N bond; ii) electrostatic coupling cannot be excluded in the pyridazyl compound (e.g., lone pair repulsion within the N=N moiety may be mitigated by the S···N interactions), which would favor rigidity and overall π-electron conjugation; iii) strengthening of these S···N interactions (see Figure 8) could decouple the S electron pair from the thiophene $4n+2$ ring aromaticity, thus favoring inter-ring conjugation. These concurrent effects are evident in the optical spectra through a red-shift of the lowest energy absorption transition on going from **1**→**2**.

As already mentioned, upon excitation of the HOMO–LUMO transition, the emission spectra of the longer oligothiophenes (i.e., 3–6 units) exhibit vibronic features reflecting rigidity of the quinoidal emitting S_1 state. For these excited states, the additional conjugation of the **6** fragment with the external six-membered groups accounts for the vibronic peaks in the thiophene-diazine derivatives (note that **6** does not exhibit a vibronic progression). Fluorescence quantum yields greatly increase upon conjugation of the central bithiophene fragment with the diazine groups, likely owed to the decreasing S atom role. Moreover, the solid state emission spectra are red-shifted nearly by 100 nm vs. the solution spectra, indicating strong solid state intermolecular interactions. Comparison with bithiophene in the solid state corroborates the importance of the intra/intermolecular contacts characteristic of diazines. Note that **1** displays a greater fluorescence quantum yield than **2**, likely owed to the *meta*→*para* change in connectivity with the bithienyl fragment.

Table 5 compares experimental emission energies and fluorescence quantum yields with the theoretical $S_1 \rightarrow S_0$ transition energies and oscillator strengths from TD-DFT/B3LYP/6-31G** calculations on **1**–**6**, using RCIS S_1 geometries. For radiative decay processes from the first excited singlet, oscillator strengths in the S_1 geometry are proportional to the decay radiative constant k_{rad} and consequently, for molar extinction coefficients and $S_0 \rightarrow S_1$ oscillator strengths in absorption, theoretical and experimental comparisons can be delineated for emission.

Table 5. Comparison for experimental and calculated data for the fluorescence emission properties of molecules **1**–**6**. Theoretically the $S_1 \rightarrow S_0$ transition is considered to be the relevant radiative transition. For **3**, methyl groups rather than hexyl groups are considered in the model.

Compound	Experimental			Theoretical		
	λ_f [nm]	ΔE [eV]	Φ_f	λ_f [nm]	ΔE [eV]	f
1	455	2.72	0.38	476	2.60	1.68
2	465	2.67	0.24	509	2.44	1.99
3	455	2.72	0.42	478	2.59	1.79
4	505*, 539	2.46	0.46	566	2.19	2.09
5	450*, 478	2.76	0.20	484	2.56	1.27
6	363	3.42	0.01	351	3.54	0.44

The maxima of the emission bands for molecules **1**–**6** follow the same trend as the theoretical $S_1 \rightarrow S_0$ transition energies. Theoretical and experimental Stokes shifts also exhibit the same trends. From **1** to **3**, the fluorescence quantum yields slightly increase, as do the associated oscillator strengths. Also, for the homologous oligothiophene series, $S_1 \rightarrow S_0$ oscillator strengths and fluorescence quantum yields behave similarly. For **6**, discrepancies between experiment and theory are observed, likely due to efficient intersystem crossing, not considered in the calculations, and which has been reported for the shortest member.[75] From **1** to **2**, Φ_f decreases (0.38 and 0.24), whereas the computation predicts an increase of the oscillator strength (1.68 and 1.99).

The above comparisons establish that a main route of relaxation from the S_1 excited states in larger oligothiophenes is a radiative process, involving dipole–dipole coupling between the two electronic states. This is important since the photophysical properties of aromatic oligothiophenes are affected by other fluorescence quenching processes, namely intersystem crossing for short chain molecules such as mentioned above for **6**. In this regard, the fluorescence quantum yield of **2** deviates from the theoretical prediction and is likely affected by intersystem crossing. To some extent the *para* connectivity of the pyridazyl moiety more efficiently involves N atom participation in the π-electron system, and heteroatoms always favor non-radiative decay routes such as intersystem crossing or charge transfer processes.[76] One additional reason is evident in Figure 9 in which S_1 state geometrical distortions are shown. Note that, evolving from S_0 to S_1, **2** always exhibits smaller C–C changes, as in the common bithiophene fragment. This implies that π-electron delocalization is reduced compared to the two homologues, and therefore intersystem crossing is more probably owed to greater conformational flexibility.

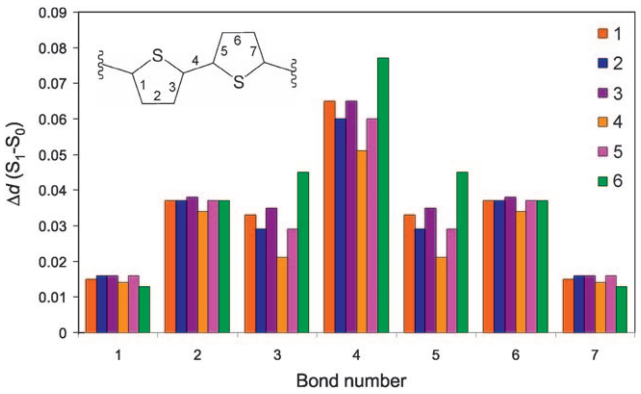

Figure 9. The C–C bond distance differences between the S_0 and S_1 states for the compounds under study.

Figure 9 presents RCIS/3-21G* ab initio optimized geometries for the S_1 states of **1**–**6**. Note that the skeletal backbone is partially quinoidal and planar in the ground electronic state. Averaged skeletal deformations and hence ri-

gidity in the **1**–**3** molecules are always midway between those observed for **5** and **4**. This rigidity likely justifies the larger computed $S_1 \rightarrow S_0$ oscillator strengths (1.68 in **1**) compared to $S_0 \rightarrow S_1$ (1.62 in **1**), the small difference can be attributed to the existing core stiffening in S_0 by S···N interactions. In this regard, the greater Φ_f in **1** vs. **2** can be also argued to result from the stronger through-space S···N interactions in the former (e.g., the larger computed rotational barriers in Figure 8). This result is significant since it demonstrates that for molecules with the same or similar numbers of π-electrons, core rigidity enhances emissive properties.

Thin film characterization: Organic semiconductor film microstructure characterization is essential to understanding charge transport in OFETs and other semiconductor-based devices. For OFETs, critical factors are semiconductor film crystallinity, molecular orientation with respect the dielectric surface, crystal grain size and connectivity, and how these properties are affected by the surface chemistry of the substrate on which the semiconductor film is deposited. Films of the new semiconductors (50 nm thick) were deposited by thermal evaporation under high vacuum on glass substrates and p^{++}-Si wafers havinga 300 nm thick thermal oxide coating. Semiconductor film crystallinity and molecular orientation on the dielectric surface were assessed by wide-angle x-ray diffraction (WAXRD) measurements. Organic semiconductor film morphology was studied by scanning electron microscopy (SEM).

WAXRD θ–2θ diffraction patterns of the thiophene-diazine films deposited at the optimized temperature $T_D =$ 110 °C indicate that all films are poorly textured (Figure 10). Films deposited at lower temperatures ($T_D = 25$, 70, 90 °C, not shown) exhibit weaker/broader Bragg reflections indicative of lower crystallinity. The diffraction pattern of **1** indicates the presence of only a single phase characterized by a d-spacing of ≈22 Å (1st through 4th order reflections observed). However, the XRD intensity of this film is far weaker than that of 50 nm thick films of **4** and other oligothiophenes. The diffraction pattern for **2** exhibits two phases/orientations, one of which dominates. This high-intensity phase is characterized by a d-spacing of 19.9 Å, versus a d-spacing of 21.7 Å for the low-intensity phase. However, the reflections of both phases are quite broad, suggesting minimal microstructural order. From the computed **1** and **2** molecular lengths (Table 6) and the corresponding d-spacings for the dominant phase, the average molecular tilt angles with respect the substrate normal are estimated to be ≈32° and ≈42°, respectively. Note that these angles are somewhat larger than those found for **4** films (≈28°). The **3** films are also composed of a mixture of two phases or orientations. The majority phase/orientation exhibits a d-spacing of 27.3 Å, whereas the other phase/orientation is characterized by an unusually small d-spacing of 18.6 Å. The corresponding molecular tilt angles for the two phases are estimated to be ≈45° and ≈61°, respectively. SEM images of the present semiconductor films deposited at 110 °C show that all films are polycrystalline with the **3** films exhibiting the largest crystallites (Figure 11). Compounds **1** and **2** film crystallites are ≈50 nm wide by 200–300 and 50–150 nm in length, respectively. The surface of **3** reveals a smooth background and the presence of large ribbon-like flakes ≈1 μm in size. Similar morphologies have been observed for several oligothiophene films and are generally favorable for efficient carrier mobility.[77]

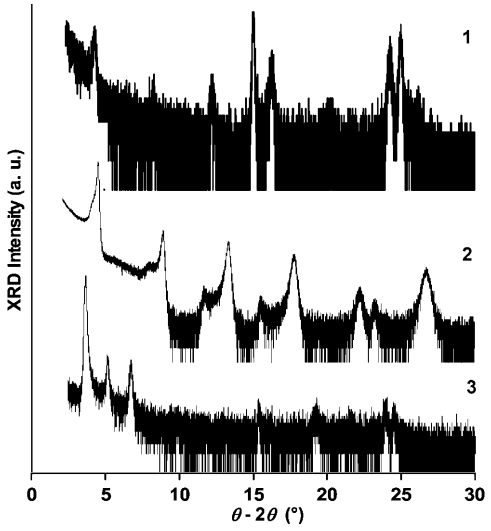

Figure 10. WAXRD $\theta-2\theta$ diffraction patterns of 50 nm semiconductor films vapor-deposited onto HMDS-treated Si/SiO_2 substrates at 110 °C. The intensity of the first reflection is: 850 (**1**), 109400 (**2**), and 20300 cps (**3**).

Table 6. Observed *d* spacing values and computed/experimental geometric parameters for films of compounds **1**–**6**.

Compound	*D* spacing [Å]	Molecular Length [Å][a,b]
1	22.0	25.87
2	19.9, 21.7	26.75
3	27.3, 18.6	38.82
4	23.3	26.59 (26.14)
5	15.43	18.75 (18.17)
6	7.82	10.90 (10.61, 10.90)

[a] Both lengths include van der Waals radii for carbon (1.70 Å) and hydrogen atoms (1.20 Å). [b] Numbers in parentheses indicate experimental values from single crystal X-ray structures (see Ref. [68]).

Transistor characterization: The semiconductor performance of the present new materials was evaluated in a top-contact bottom-gate OFET geometry. All of the new materials exhibit p-type transport. Compound **2** exhibits the highest mobility of 4×10^{-3} $cm^2 V^{-1} s^{-1}$, a threshold voltage $V_T = -68$ V, and current on off ratio $I_{on:off} = 10^7$ for films grown at $T_D =$ 110 °C. In general, these saturation hole mobilities (μ_h) are greater for films grown on hexamethyldisilazane (HMDS)-treated substrates (Table 7) than on bare SiO_2. Interestingly, electron transport is not observed for these devices, although the diazine-thiophene semiconductors are clearly

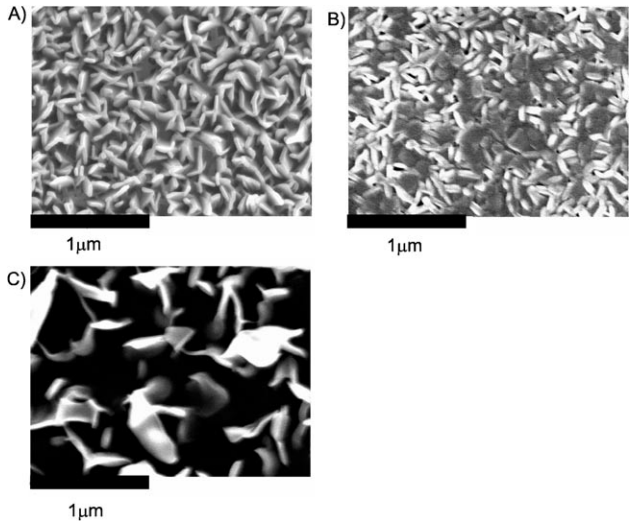

Figure 11. Scanning electron micrographs of films of the thiophene-diazine semiconductors A) **1**, B) **2**, and C) **3** vapor-deposited onto HMDS-treated SiO_2/Si at 110 °C.

more electron-deficient than their p-type oligothiophene analogues (see the Electrochemistry Section).

The alkyl-substituted pyrimidine **3** exhibits μ_h comparable to that of **2** for most growth temperatures, with optimized parameters $\mu_h = 3\times10^{-3}\,cm^2V^{-1}s^{-1}$, $V_T = -55$ V, and $I_{on:off} = 2\times10^7$. Note that the μ_h variations observed over a 85 °C growth range can be considered inconsequential for a material having mobilities in this range. The **3** films have similar μ_h values on both hydrophobic and hydrophilic substrates. These observed μ_h variations may reflect small differences in charge carrier trap densities and/or local film morphology variations. The unsubstituted pyrimidine semiconductor **1** exhibits far lower μ_h values and exhibits significant sensitivity to the dielectric surface energy. Thus, μ_h on the bare hydrophilic SiO_2 surface is typically 10^3 times lower than on HMDS-treated substrates, and hole transport is not observed for 25 °C growth on untreated SiO_2. Increased substrate sensitivity and lower μ_h has been observed previously for unfunctionalized thiophenes such as **5** and **4**.[36]

The greater μ_h observed in **2** is likely a result of a more linear geometry, as shown by the TD-DFT calculations. In this material, a pyrazine fragment joins two thiophenes through *para* connections as opposed to pyrimidines in **1** and **3**, which are *meta* functionalized. This *meta* functionalization results in non-linear ring-ring connections, each of which can have two conformations, which are computed to lie within 1 kcal mol^{-1} (Figure 8). Such energetically similar conformations may create packing defects that would lower the observed μ_h.

Charge transport vs. molecular structure: We conclude by discussing OFET charge transport trends, analyzing thiophene-azine molecular electronic and structural parameters, such as redox properties and intramolecular reorganization energies (i.e., λ_h). The latter parameter considers the structural reorganization needed to accommodate charge as a prerequisite for efficient transport. These λ_h parameters, computed as described in literature,[78] are compiled in Table 8 together with the experimental electrochemical oxidation potentials E_{ox1} and OFET hole mobilities. With the exception of **2**, reorganization energies for anions which are the molecular parameter relevant to electron transport in these materials are larger than those predicted for cations. The *n*-hexyl substitution of **1** in **3** decreases the hole reorganization energy by 0.03 eV, in agreement with the observed increase in p-type mobility. In the case of **4** and **5** versus the diazine molecules, the greater hole mobility appears to be aided by more facile hole formation (i.e., lower E_{ox1}) although the small reorganization energies in the diazines suggest that mobilities should be similar. The FET mobility of **6** has not been reported. The present semiconductor description is in accord with the above discussion of the op-

Table 8. Reorganization energies, oxidation potentials, and maximum hole mobilities measured for compounds **1**–**5**.

Compound	$\lambda_{h(radical\ anion)}$ [eV]	$\lambda_{h(radical\ cation)}$ [eV]	E_{ox1} [V]	μ_H [cm^{2}V^{-1}s^{-1}]
1	0.2751	0.2468	1.63	1×10^{-4}
2	0.2312	0.2353	1.87	4×10^{-3}
3	0.3009	0.2192	1.60	3×10^{-3}
4	–	0.301[a]	0.98	6×10^{-2}
5	–	0.345[a]	1.10	1×10^{-2}

[a] Values are taken from reference [78].

Table 7. FET mobilities (μ, cm^{2}V^{-1}s^{-1}), current on:off ratios (I_{on}:I_{off}), and threshold voltages (V_T, V) for semiconductor films of series **1**–**5**, as a function of deposition temperature.

Compound	Sbs.[a]	25 °C			70 °C			90 °C			110 °C		
		μ	I_{on}:I_{off}	V_T	μ	I_{on}:I_{off}	V_T	μ	I_{on}:I_{off}	V_T	μ	I_{on}:I_{off}	V_T
1	S	NA	NA	NA	3×10^{-7}	3×10^{2}	−70	8×10^{-7}	1×10^{3}	−124	2×10^{-6}	6×10^{3}	−85
	H	2×10^{-5}	5×10^{3}	−84	1×10^{-4}	2×10^{5}	−88	1×10^{-4}	1×10^{4}	−97	3×10^{-5}	3×10^{4}	−80
2	S	3×10^{-4}	1×10^{4}	−67	1×10^{-3}	1×10^{6}	−87	1×10^{-4}	4×10^{5}	−107	2×10^{-3}	1×10^{5}	−64
	H	2×10^{-3}	2×10^{5}	−77	2×10^{-3}	1×10^{7}	−74	8×10^{-4}	2×10^{5}	−82	4×10^{-3}	1×10^{7}	−68
3	S	3×10^{-4}	1×10^{5}	−90	4×10^{-5}	1×10^{5}	−66	1×10^{-4}	2×10^{4}	−85	2×10^{-5}	3×10^{4}	−103
	H	2×10^{-4}	2×10^{5}	−43	7×10^{-4}	3×10^{6}	−106	3×10^{-3}	2×10^{7}	−55	2×10^{-4}	1×10^{5}	−99
4	H	4×10^{-2}	2×10^{4}	−14	6×10^{-2}	4×10^{4}	−12	3×10^{-2}	1×10^{4}	−10			
5	H	1×10^{-2}	1×10^{5}	−17	1×10^{-2}	1×10^{5}	−15	5×10^{-3}	7×10^{4}	−18			

[a] Substrate surface treatment; S: SiO_2, H: HMDS.

tical spectroscopy and electrochemistry which indicate that a significant portion of thiophene-diazine properties is dominated by the central bithiophene fragment. The role of the diazine units thus appears largely to extend the intrinsic characteristics of the bithienyl units but, as a whole, not to introduce unique electronic properties. In this sense, these extended bithiophenes counter-intuitively behave as conventional hole-semiconducting oligothiophenes with properties similar to those of medium-sized oligothiophenes (i.e., 3–4 thiophene units).

Conclusions

Three new diazine-functionalized oligothiophenes have been synthesized and their structural, optical, vibrational, electrochemical, and semiconductor properties studied in comparison with those of the corresponding oligothiophenes, with the goal of enhancing transport properties of value in organic electronics. The molecular properties of these systems are dominated by the central bithiophene fragment, and hence their properties correspond largely to π-electron extended bithiophenes. This is surprising in the case of charge mobility since, a priori, these materials would appear to be best suited for electron transport (i.e., azine units behave as electron acceptors). These diazine-functionalized oligothiophenes are reasonably efficient hole transporters, an innate characteristic of readily oxidized oligothiophenes. To probe these issues further, a broad set of interconnected physicochemical data (optical, electrochemical, vibrational, conformational, energetic, etc.) are acquired and analyzed. Regarding organic electronics, the present diazine-oligothiophene OFET mobilities are moderate. Further work will focus on modification of azine synthons, for example with electron acceptors, which could effect majority charge carrier sign inversion, or even more interesting, afford ambipolar semiconductors able to transport in a similar regime, holes (owing to the bithiophene portion) and electrons (owing to the azine units). Such charge transport characteristics, if properly combined with emissive properties, may provide new OLET materials combining electron-hole transport with efficient luminescence.

Experimental Section

Materials and methods: The reagents 5,5′-bis(tri-*n*-butylstannyl)-2,2′-bithiophene and 2-(tri-*n*-butylstannyl)thiophene were synthesized according to known procedures.[79] The reagent 2-(tri-*n*-butylstannyl)-5-hexylthiophene was synthesized as reported earlier.[80] ^{1}H NMR (400 MHz) spectra were measured in $CDCl_3$ or CD_2Cl_2 on a Varian Mercury 400 (room temperature) or a Varian Inova 400 (high temperature) instrument.

Synthesis of 4,6-dithien-2-ylpyrimidine (9):[81] A mixture of 2-tri-*n*-butylstannylthiophene (10.52 g, 28.19 mmol), 4,6-dichloropyrimidine (2.00 g, 13.42 mmol), tetrakis(triphenylphosphine)palladium(0) (0.345 g, 0.30 mmol), and a few crystals of 2,6-di-*tert*-butyl-4-methylphenol in dry toluene (20 mL) was deaerated twice with nitrogen. The reaction mixture was then refluxed for 6 h and, after cooling, a white precipitate formed in the reaction flask. The crude solid product was removed by filtration, and the filtrate was diluted with ether (100 mL), poured into an aqueous solution of $NH_4^+F^-$ (3.0 g, 100 mL), and the organic phase separated. After drying over $MgSO_4$ and filtration, the solvent was evaporated affording a white solid. The two solid portions were next combined and recrystallized from toluene to give the pure product as a colorless crystals (2.36 g, 9.66 mmol, 72.0% yield). M.p. = 146 °C; ^{1}H NMR ($CDCl_3$): δ = 9.07 (d, ^3J = 1.4 Hz, 1H), 7.86 (d, ^3J = 3.7 Hz, 1H), 7.83 (d, 1H), 7.57 (d, ^3J = 5.1 Hz, 1H), 7.20 ppm (dd, 1H).

Synthesis of 5,5′-bis-(6-chloropyrimid-4-yl)-2,2′-dithiophene (7): A mixture of 5,5′-bis(tri-*n*-butylstannyl)-2,2′-dithiophene (7.58 g, 10.18 mmol), 4,6-dichloropyrimidine (6.00 g, 40.27 mmol) and tetrakis(triphenylphosphine)palladium(0) (0.26 g, 0.22 mmol) in dry toluene (70 mL) was deaerated twice with nitrogen. The reaction mixture was next refluxed for 6 h and, after cooling, the resulting precipitate was collected by filtration. The crude solid product was washed several times with hexane and then with methanol, to afford the essentially pure product as a yellow powder (2.80 g, 7.16 mmol, 70.3% yield). M.p. = 261 °C (sublimation); ^{1}H NMR ($CDCl_3$): δ = 8.91 (d, ^3J = 1.3 Hz, 2H), 7.73 (d, ^3J = 4.0 Hz, 2H), 7.60 (d, 2H), 7.37 ppm (d, 2H); MS(70 eV): *m*/*z* (%): 390.9(100%) 392.9 (75%); elemental analysis calcd (%) for $C_{16}H_8Cl_2N_4S_2$: C 49.11 ,H 2.06, N 14.32; found: C 49.21, H 2.19, N 14.16.

Synthesis of 5,5′-bis(6-(thien-2-yl)pyrimid-4-yl)-2,2′-dithiophene (1): A mixture of 5,5′-bis(6-chloropyrimid-4-yl)-2,2′-dithiophene (1.40 g, 3.58 mmol), tri-*n*-butylstannylthiophene (3.00 g, 8.04 mmol), tetrakis(triphenylphosphine)palladium(0) (0.20 g, 0.17 mmol), and few crystals of 2,6-di-*tert*-butyl-4-methylphenol in dry toluene (120 mL) was deaerated twice with nitrogen. The reaction mixture was then refluxed for 10 h and, after cooling, the precipitate was collected by filtration (2.00 g). The solid residue was washed several times with hexane and then recrystallized from pyridine (170 mL) to afford the pure product as an orange solid (0.88 g, 1.81 mmol, 50.5% yield). Extremely pure samples can be obtained by gradient sublimation. mp = 306 °C; ^{1}H NMR ($CDCl_3$): δ = 9.09 (d, ^3J = 1.2 Hz, 2H), 7.94 (d, ^3J = 3.7 Hz, 2H), 7.85 (d, ^3J = 4.0 Hz, 2H), 7.83 (d, 2H), 7.61 (d, ^3J = 4.9 Hz, 2H), 7.41 (d, 2H), 7.24 (dd, 2H); MS-(70 eV): *m*/*z* (%): 487.0 (100); elemental analysis calcd (%) for $C_{24}H_{14}N_4S_4$: C 59.23, H 2.91, N 11.52; found: C 59.17, H 2.97, N 11.37.

Synthesis of 5,5′-bis(6-(5-hexylthien-2-yl)pyrimid-4-yl)-2,2′-dithiophene (3): A mixture of 5,5′-bis(6-chloropyrimid-4-yl)-2,2′-dithiophene (1.05 g, 2.68 mmol), 2-(tri-*n*-butylstannyl)-5-hexylthiophene (2.60 g, 5.68 mmol), tetrakis(triphenylphosphine)palladium(0) (0.15 g, 0.13 mmol), and few crystals of 2,6-di-*tert*-butyl-4-methylphenol in dry toluene (90 mL) was deaerated twice with nitrogen. The reaction mixture was then refluxed for 12 h and, after cooling, the precipitate was collected by centrifugation (1.66 g). The solid crude product was washed once with hexane and then dissolved in hot chloroform (150 mL). The warm solution was filtered and the solvent evaporated to give the pure product as a brown solid (1.21 g, 1.85 mmol, 71.1% yield). An analytically pure sample was obtained by recrystallization from toluene. M.p. = 230 °C; ^{1}H NMR ($CDCl_3$): δ = 9.04 (d, ^3J = 1.1 Hz, 2H), 7.78 (d, ^3J = 4.0 Hz, 2H), 7.72 (d, ^3J = 3.8 Hz, 2H), 7.83 (d, 2H), 7.37 (d, ^3J = 4.2 Hz, 2H), 6.90 (d, 2H), 2.89 (t, ^3J = 7.5 Hz, 4H), 1.76 (m, 4H), 2.00–1.40 (m, 12H), 0.91 ppm (t, ^3J = 7.3 Hz, 6H); elemental analysis calcd (%) for $C_{36}H_{38}N_4S_4$: C 66.01, H 5.86, N 8.56; found: C 65.88, H 5.57, N 8.57.

Synthesis of 3-(thien-2-yl)-6-chloropyridazine (8):[82] A mixture of tri-*n*-butylstannylthiophene (6.26 g, 16.78 mmol), 3,6-dichloropyridazine (5.00 g, 33.56 mmol), tetrakis(triphenylphosphine)palladium(0) (0.20 g, 0.17 mmol), and few crystals of 2,6-di-*tert*-butyl-4-methylphenol in DMF (50 mL) was deaerated twice with N_2. The reaction mixture was then heated at 80 °C for 6 h and, after cooling, poured into water (100 mL). The resulting white precipitate was collected, washed several times with water, and dried under vacuum. This solid was next taken up in ether (25 mL) and filtered to afford nearly pure solid product (3.01 g, 36.7% yield) after evaporation of the ether. Finally, this solid was recrystallized from MeOH-H_2O to give the pure target compound as white crystals (1.56 g, 7.90 mmol, 47.3% yield). M.p. = 155 °C; ^{1}H NMR ($CDCl_3$): δ = 7.75 (d, ^3J = 11.0, 1H), 7.68 (d, ^3J = 3.6, 1H), 7.54 (d, ^3J = 5.0, 1H), 7.51 (d, 1H), 7.18 ppm (dd, 1H).

Synthesis of 5,5′-bis(6-(thien-2-yl)pyridazin-3-yl))-2,2′-dithiophene (2): A mixture of 3-(thien-2-yl)-6-chloropyridazine (1.50 g, 7.63 mmol), 5,5′-bis(tri-*n*-butylstannyl)-2,2′-dithiophene (2.84 g, 3.81 mmol), and tetrakis-(triphenylphosphine)palladium(0) (0.09 g, 0.08 mmol) in dry DMF (30 mL) was deaerated twice with nitrogen. The reaction mixture was then heated at 70 °C overnight. After cooling, the resulting precipitate was collected and washed several times with hexane, MeOH, and ether. After drying, the pure product was obtained as a light-orange solid (1.60 g, 3.29, 86.3 % yield). M.p. > 350 °C; elemental analysis calcd (%) for $C_{24}H_{14}N_4S_4$: C 59.23, H 2.91, N 11.52; found: C 58.85, H 3.11, N 11.57. NMR experiment was not recorded, owing to the low solubility of this compound. However the elemental analysis and mass allowed us to assess the compounds identity and purity.

Raman and optical spectroscopic measurements: FT-Raman scattering spectra were collected on a Bruker FRA106/S instrument with a Nd:YAG laser source ($\lambda_{exc} = 1064$ nm), in a back-scattering configuration. The operating power for the exciting radiation was limited to 100 mW in all the experiments. Samples were analyzed as pure solids, averaging 1000 scans with 4 cm^{-1} spectral resolution. Raman spectra of thin films were recorded using a RENISHAW Microscope Invia Reflex Raman working with the 514.5 nm laser excitation wavelength. UV/Vis absorption spectra were collected on an Agilent 8453 instrument equipped with a diode array for the fast acquisition of all absorptions in the 190–1100 nm spectral range. Fluorescence spectra were recorded with a Jasco FP-750 spectrometer. Solutions were prepared with an absorbance between 0.1 and 0.2 at the wavelength region of experimental interest. Fluorescence quantum yields were determined by comparison with 0.1 M quinine sulfate in 0.05 M sulfuric acid as reference and corrected for the refractive index of the solvent.

Electrochemical measurements: Cyclic voltammetry experiments were performed in 0.1 M tetrabutyl ammonium hexafluorophosphate ($TBAPF_6$) solutions in dry, oxygen-free THF. Glassy carbon was used as the working electrode, platinum gauze as the auxiliary electrode, and Ag/AgCl as the reference electrode, which was checked against the Fc/Fc^+ couple after each measurement.

Thermal measurements: Differential scanning calorimetry (DSC) and thermogravimetric analysis (TGA) were performed by using TA DSC 2920 and Mettler–Toledo TGA instruments, respectively.

Thin film growth, characterization, and device fabrication: Prime grade p-doped silicon wafers (100) of 300 nm thermally grown oxide (Process Specialties Inc. and Montco Silicon Technologies Inc.) were used as device substrates. They were first rinsed with water, methanol, and acetone before film deposition. Trimethylsilation of the Si/SiO_2 surface was carried out by exposing the silicon wafers to HMDS vapor at room temperature in a closed container under N_2 overnight. Organic semiconductors were deposited by vacuum evaporation (pressure $< 10^{-5}$ Torr) at selected substrate temperatures and at a growth rate of 0.2–0.3 Å s^{-1}. Evaporated films were 500 Å thick (as determined by a calibrated in situ quartz crystal monitor). For FET device fabrication, top-contact electrodes (500 Å) were deposited by evaporating gold (pressure $< 10^{-5}$ Torr); channel dimensions were 50/100 μm (L) by 5.0 mm (W). The capacitance of the insulator is 2×10^{-8} F cm^{-2} for 300 nm SiO_2. TFT device measurements were carried out in a customized high-vacuum probe station pumped down to 8×10^{-6} Torr before being backfilled with argon or air. Coaxial and/or triaxial shielding was incorporated into Signatone probe stations to minimize the noise level. TFT characterization was performed with a Keithly 6430 sub-femtoamp meter and a Keithly 2400 source meter, operated by a locally written Labview program and GPIB communication. Thin films were analyzed by using wide-angle X-ray film diffractometry (WAXRD) on a Rikagu ATX-G using standard θ-2θ techniques, with monochromated CuKα radiation. All θ-2θ scans were calibrated in situ using the Si (100) substrate reflections.

Computational methods: Density functional theory (DFT) calculations were carried with the Gaussian 03[83] program running on an SGI Origin 2000 supercomputer. Becke's three-parameter exchange functional combined with the LYP correlation functional (B3LYP) was used.[84] It is known that the B3LYP functional yields similar geometries for medium-sized molecules as do MP2 calculations with the same basis sets.[85] Moreover, DFT force fields calculated using the B3LYP functional yield infrared spectra in very good agreement with experiment.[86] The standard 6-31G** basis set was used.[87] Optimized molecular geometries were determined on isolated entities. Vertical one-electron excitations were computed using time-dependent DFT (TDDFT) methods.[88] The 20 lowest-energy electronic excited states were computed for **1** and **2**. The geometry optimization of the first excited S_1 state was carried out using ab initio methods with restricted configuration interaction singles (RCIS) incorporated in Gaussian 03,[89] and the 3–21G* basis was chosen for all molecules. TD-DFT/B3LYP/6-31G* calculations were used to calculate $S_1 \rightarrow S_0$ electronic transition frequency from the optimized (relaxed) S_1 state. These calculations were performed over the geometries optimized by RCIS method.

Acknowledgements

We thank ONR (N00014–02–0909), the NSF-MRSEC program through the Northwestern Materials Research Center (DMR-0520513), and Polyera Corporation for support of this research at Northwestern. Research at the University of Malaga was supported by the Ministerio de Educacion y Ciencia (MEC) of Spain through Project CTQ2006-14987-C02-01. We are also indebted to the Junta de Andalucia for funding our FQM-0159 scientific group and for the Project P06-FQM-01678. R. P. O. thanks the MEC for a personal postdoctoral grant.

[1] a) *Handbook of Oligo- and Polythiophenes* (Ed.: D. Fichou), Wiley-VCH, Weinheim, **1999**; b) *Polythiophenes - Electrically Conductive Polymers* (Eds.: G. Schopf, G. Kossmehl), Springer, Berlin, **1997**.

[2] a) P. Frère, J.-M. Raimundo, P. Blanchard, J. Delaunay, P. Richomme, J.-L. Sauvajol, J. Orduna, J. Garin, J. Roncali, *J. Org. Chem.* **2003**, *68*, 5357; b) J. Z. Wang, Z. H. Zheng, H. W. Li, W. T. S. Huck, H. Sirringhaus, *Nat. Mater.* **2004**, *3*, 171; c) A. Afzali, T. L. Breen, C. R. Kagan, *Chem. Mater.* **2002**, *14*, 1742.

[3] a) P. Bäuerle, *Electronic Materials: The Oligomer Approach* (Eds.: K. Müllen, G. Egner), Wiley-VCH, Weinheim, **1998**, p. 105; b) L. Groenendaal, E. W. Meijer, J. A. J. M. Vekemans, *Electronic Materials: The Oligomer Approach* (Eds.: K. Müllen, G. Egner), Wiley-VCH, Weinheim, **1998**, p. 235; c) J. Gruber, R. W. Chia Li, I. A. Hümmelgen, *Handbook of Advanced Electronic and Photonic Materials and Devices, Vol. 8* (Ed.: H. S. Nalwa), Academic Press, San Diego, **2000**, pp. 163–184; d) H. Meng, J. Zheng, A. J. Lovinger, B.-C. Wang, P. G. Van Patten, Z. Bao, *Chem. Mater.* **2003**, *15*, 1778; e) J. L. Reddinger, J. R. Reynolds, *Adv. Polym. Sci.* **1999**, *145*, 57.

[4] a) S. C. Moratti, *Handbook of Conducting Polymers*; 2nd ed. (Eds.: T. A. Skotheim, R. L. Elsenbaumer, J. R. Reynolds), Marcel Dekker, New York, **1998**, pp. 343; b) R. D. McCullough, *Adv. Mater.* **1998**, *10*, 93.

[5] a) H. Meng, J. Zheng, A. J. Lovinger, B.-C. Wang, P. G. Van Patten, Z. Bao, *Chem. Mater.* **2003**, *15*, 1778; b) M. Mushrush, A. Facchetti, M. Lefenfeld, H. E. Katz, T. J. Marks, *J. Am. Chem. Soc.* **2003**, *125*, 9414; c) A. Facchetti, M. Mushrush, H. E. Katz, T. J. Marks, *Adv. Mater.* **2003**, *15*, 33; d) D. M. Delongchamp, S. Sambasivan, E. K. L. Fischer, P. Chang, A. R. Murphy, J. M. J. Fréchet, V. Subramanian, *Adv. Mater.* **2005**, *17*, 2340.

[6] a) M. Pasini, S. Destri, W. Porzio, C. Botta, U. Giovanella, *J. Mater. Chem.* **2003**, *13*, 807; b) M. Suzuki, M. Fukuyama, Y. Hori, S. Hotta, *J. Appl. Phys.* **2002**, *91*, 5706.

[7] D. Pisignano, M. Anni, G. Gigli, R. Cingolani, M. Zavelani-Rossi, G. Lanzani, G. Barbarella, L. Favaretto, *Appl. Phys. Lett.* **2002**, *81*, 3534.

[8] a) L. Torsi, A. J. Lovinger, B. Crone, T. Someya, A. Dodabalapur, H. E. Katz, A. Gelperin, *J. Phys. Chem. B* **2002**, *106*, 12563; b) J. Roncali, *J. Mater. Chem.* **1999**, *9*, 1875.

[9] K. Hara, M. Kurashige, Y. Dan-Oh, C. Kasada, A. Shinpo, S. Suga, K. Sayama, H. Arakawa, *New J. Chem.* **2003**, *27*, 783.

[10] G. Barbarella, *Chem. Eur. J.* **2002**, *8*, 5072.

[11] C. Xia, X. Fan, J. Loklin, R. C. Advincula, *Org. Lett.* **2002**, *4*, 2067.
[12] B. Jousselme, P. Blanchard, E. Levillain, J. Delaunay, M. Allain, P. Richomme, D. Rondeau, N. Gallego-Planas, J. Roncali, *J. Am. Chem. Soc.* **2003**, *125*, 1363.
[13] a) S. R. Forrest, *Nature* **2004**, *428*, 911; b) M. Muccini, *Nat. Mater.* **2006**, *5*, 605.
[14] For example, see: a) A. Kraft, A. C. Grimsdale, A. B. Holmes, *Angew. Chem.* **1998**, *110*, 416; *Angew. Chem. Int. Ed.* **1998**, *37*, 42; b) U. Mitschke, P. Bauerle, *J. Mater. Chem.* **2000**, *10*, 1471; c) A. J. Heeger, *Solid State Commun.* **1998**, *107*, 673; d) A. P. Kulkarmi, C. J. Tonzola, A. Babel, S. A. Jenekhe, *Chem. Mater.* **2004**, *16*, 4556; e) M. M. Richter, *Chem. Rev.* **2004**, *104*, 3003; f) N. R. Armstrong, R. M. Wightman, E. M. Gross, *Annu. Rev. Phys. Chem.* **2001**, *52*, 391; g) F. Fungo, K.-T. Wong, S.-Y. Ku, Y.-Y. Hung, A. J. Bard, *J. Phys. Chem. B* **2005**, *109*, 3984; h) H. Yan, P. Lee, N. R. Armstrong, A. Graham, G. A. Evmenenko, P. Dutta, T. J. Marks, *J. Am. Chem. Soc.* **2005**, *127*, 3172; i) I. F. Perepichka, D. F. Perepichka, H. Meng, F. Wudl, *Adv. Mater.* **2005**, *17*, 2281.
[15] a) G. Barbarella, L. Zanelli, A. Gigli, M. Mazzeo, M. Anni, A. Bongini, *Adv. Funct. Mater.* **2005**, *15*, 664; b) D. Wasserberg, P. Marsat, S. C. J. Meskers, R. A. J. Janseen, D. Beljonne, *J. Phys. Chem. B* **2005**, *109*, 4410; c) M. Rubio, M. Merchán, E. Ortí, *ChemPhysChem* **2005**, *6*, 1357; d) A. Köhler, D. Beljonne, *Adv. Funct. Mater.* **2004**, *14*, 11; e) F. Garnier, *Acc. Chem. Res.* **1999**, *32*, 209; f) J. Cornil, D. A. dos Santos, X. Crispin, R. Silbey, J. L. Brédas, *J. Am. Chem. Soc.* **1998**, *120*, 1289; g) R. S. Becker, J. Seixas de Melo, A. L. Macanita, F. Elisei, *J. Phys. Chem.* **1996**, *100*, 18683; h) D. Grebner, H. Helbig, S. Rentsch, *J. Phys. Chem.* **1995**, *99*, 16991; i) A. J. Janssen, L. Smilowitz, S. N. Sariciftci, D. Moses, *J. Chem. Phys.* **1994**, *101*, 1787; j) S. Hotta, K. Waragai, *J. Phys. Chem.* **1993**, *97*, 7427; k) P. Garcia, J. M. Pernaut, P. Happiot, V. Wintgens, P. Valat, F. Garnier, D. Delabouglise, *J. Phys. Chem.* **1993**, *97*, 513; l) D. Birnbaum, D. Fichou, B. Kohler, *J. Chem. Phys.* **1992**, *96*, 165.
[16] M. Ichikawa, R. Hibino, M. Inoue, T. Haritani, S. Hotta, K.-I. Araki, T. Koyama, Y. Taniguchi, *Adv. Mater.* **2005**, *17*, 2073.
[17] a) M. Ichikawa, R. Hibino, M. Inoue, T. Haritani, S. Hotta, T. Koyama, Y. Taniguchi, *Adv. Mater.* **2003**, *15*, 213; b) M. Nagawa, R. Hibino, S. Hotta, H. Yanagi, M. Ichikawa, T. Koyama, Y. Taniguchi, *Appl. Phys. Lett.* **2002**, *80*, 544.
[18] a) H. Meng, J. Zheng, A. J. Lovinger, B.-C. Wang, G. P. Van Patten, Z. Bao, *Chem. Mater.* **2003**, *15*, 1778; b) K. T. Wong, C.-F. Wang, C. H. Chou, Y. O. Su, G.-H. Lee, S. M. Peng, *Org. Lett.* **2002**, *4*, 4429.
[19] a) T. Noda, I. Imae, N. Noma, Y. Shirota, *Adv. Mater.* **1997**, *9*, 239; b) T. Noda, H. Ogawa, N. Noma, Y. Shirota, *Adv. Mater.* **1997**, *9*, 720; c) T. Noda, H. Ogawa, N. Noma, Y. Shirota, *Appl. Phys. Lett.* **1997**, *70*, 699; d) T. Noda, H. Ogawa, N. Noma, Y. Shirota, *J. Mater. Chem.* **1999**, *9*, 2177.
[20] a) Y. Shirota, M. Kinoshita, T. Noda, K. Okumoto, O. Takahiro, *J. Am. Chem. Soc.* **2000**, *122*, 11021; b) H. Doi, M. Kinoshita, K. Kumoto, Y. Shirota, *Chem. Mater.* **2003**, *15*, 1080.
[21] a) H. Akimichi, K. Waragai, S. Hotta, H. Kano, H. Sakaki, *Appl. Phys. Lett.* **1991**, *58*, 1500; b) F. Garnier, A. Yassar, R. Hajlaoui, G. Horowitz, F. Deloffre, B. Servet, S. Ries, P. Alnot, *J. Am. Chem. Soc.* **1993**, *115*, 8716; c) H. E. Katz, L. Torsi, A. Dodabalapur, *Chem. Mater.* **1995**, *7*, 2235; d) H. E. Katz, *J. Mater. Chem.* **1997**, *7*, 369.
[22] a) A. Tsumara, H. Koezuka, T. Ando, *Appl. Phys. Lett.* **1986**, *49*, 1210; b) A. Assadi, C. Svensson, M. Willander, O. Inganäs, *Appl. Phys. Lett.* **1988**, *53*, 195.
[23] a) C. D. Dimitrakopoulos, B. K. Furman, T. Graham, S. Hedge, S. Purushothaman, *Synth. Met.* **1998**, *92*, 47; b) H. E. Katz, A. J. Lovinger, J. G. Laquindanum, *Chem. Mater.* **1998**, *10*, 457; c) H. E. Katz, J. G. Laquindanum, A. J. Lovinger, *Chem. Mater.* **1998**, *10*, 633; d) M. Halik, H. Klauk, U. Zschieschang, G. Schmid, S. Ponomarenko, S. Kirchmeyer, W. Weber, *Adv. Mater.* **2003**, *15*, 917; e) D. M. Delongchamp, B. M. Vogel, Y. Jung, M. C. Gurau, C. A. Richter, O. A. Kirillov, J. Obrzut, D. A. Fischer, S. Sambasivan, L. J. Richter, E. K. Lin, *Chem. Mater.* **2005**, *17*, 5610; f) P. M. Delongchamp, R. J. Kline, E. K. Lin, D. A. Fischer, L. J. Richter, L. A. Lucas, M. Heeney, I. McCulloch, J. E. Northrup, *Adv. Mater.* **2007**, *19*, 833.
[24] a) A. Facchetti, M.-H. Yoon, T. J. Marks, *Adv. Mater.* **2005**, *17*, 1705; b) J. Veres, S. Ogier, G. Lloyd, D. de Leeuw, *Chem. Mater.* **2004**, *16*, 4543; c) D. M. Delongchamp, B. M. Vogel, Y. Jung, M. C. Gurau, C. A. Richter, O. A. Kirillov, J. Obrzut, D. A. Fischer, S. Sambasivan, L. J. Richter, E. K. Lin, *Chem. Mater.* **2005**, *17*, 5610.
[25] a) H. Fukumoto, A. Kumagai, Y. Fujiwara, H. Koinuma, T. Yamamoto, *Heterocycles* **2006**, *68*, 1349; b) T. Yasuda, Y. Sakai, S. Aramaki, T. Yamamoto, *Chem. Mater.* **2005**, *17*, 6060; c) G. Sonmez, C. K. F. Shen, Y. Rubin, F. Wudl, *Adv. Mater.* **2005**, *17*, 897; d) L. M. Campos, A. Tontcheva, S. Gunes, G. Sonmez, H. Neugebauer, N. S. Sariciftci, F. Wudl, *Chem. Mater.* **2005**, *17*, 4031; e) R. D. Champion, K.-F. Cheng, C.-L. Pai, W.-C. Chen, S. A. Jenekhe, *Macromol. Rapid Commun.* **2005**, *26*, 1835; f) A. K. Agrawal, S. A. Jenekhe, *Macromolecules* **1993**, *26*, 895; g) Y. Cui, X. Zhang, S. A. Jenekhe, *Macromolecules* **1999**, *32*, 3824; h) M. Svensson, F. Zhang, S. C. Veenstra, W. J. H. Verhees, J. C. Hummelen, J. M. Kroon, O. Inganäs, M. R. Andersson, *Adv. Mater.* **2003**, *15*, 988.
[26] *Handbook of Organic Conductive Molecules and Polymers, Vol. 2–4* (Ed.: H. S. Nalva), Wiley, New York, **1997**.
[27] a) J. Krajcovic, G. Cik, D. Végh, F. Sersen, *Synth. Met.* **1999**, *105*, 79; b) G. Cík, J. Krajcovic, P. Veis, D. Végh, F. Sersen, *Synth. Met.* **2001**, *118*, 111.
[28] A. I. Khodair, P. Bertrand, *Tetrahedron* **1988**, *44*, 4859.
[29] E. E. Schweizer, A. L. Rheingold, M. Bruch, *J. Org. Chem.* **1993**, *58*, 4339.
[30] a) R. Centore, C. Garzillo, *J. Chem. Soc. Perkin Trans. 1* **1997**, *22*, 79; b) P. Espinet, J. Etxebarria, M. Marcos, J. Péres, A. Remón, J. L. Serrano, *Angew. Chem.* **1989**, *101*, 1076; *Angew. Chem. Int. Ed. Engl.* **1989**, *28*, 1065.
[31] H. S. Nalwa, A. Kakatu, A. Mukoh, *J. Appl. Phys.* **1993**, *73*, 4743.
[32] M. X. Hong, H. E. Katz, A. J. Lovinger, B.-C. Wang, K. Raghavachari, *Chem. Mater.* **2001**, *13*, 4686.
[33] a) Y. Zhu, R. D. Champion, S. A. Jenekhe, *Macromolecules* **2006**, *39,* 8712; b) R. D. Champion, K.-F. Cheng, C.-L. Pai, W.-C. Chen, S. A. Jenekhe, *Macromol. Rapid Commun.* **2005**, *26*, 1835; c) T. Yamamoto, T. Yasuda, Y. Sakai, S. Aramaki, *Macromol. Rapid Commun.* **2005**, *26*, 1214.
[34] a) A. Abbotto, S. Bradamante, A. Facchetti, G. A Pagani, *J. Org. Chem.* **2002**, *67*, 5753; b) K. B. Wiberg, T. P. Lewis, *J. Am. Chem. Soc.* **1970**, *92*, 7154.
[35] a) S. Sharma, D. Lacey, P. Wilson, *Liq. Cryst.* **2003**, *30*, 461; b) P. Liu, H. Nakano, Y. Shirota, *Liq. Cryst.* **2001**, *28*, 581; c) R. Azumi, G. Götz, P. Bäuerle, *Synth. Met.* **1999**, *101*, 544.
[36] a) A. Facchetti, M.-H. Yoon, C. L. Stern, G. R. Hutchison, M. A. Ratner, T. J. Marks, *J. Am. Chem. Soc.* **2004**, *126*, 13480; b) A. Zen, M. Saphiannikova, D. Neher, J. Grenzer, S. Grigorian, U. Pietsch, U. Asawapirom, S. Janietz, U. Scherf, I. Lieberwirth, G. Wegner, *Macromolecules* **2006**, *39*, 2162.
[37] J. Jagur-Grodzinski, *Polym. Adv. Technol.* **2002**, *13*, 615.
[38] a) W. Domagala, M. Laokowski, S. Guillerez, G. Bidan, *Electrochim. Acta* **2003**, *48*, 2379; b) K. Meerholz, J. Heinze, *Electrochim. Acta* **1996**, *41*, 1839.
[39] J. Jagur-Grodzinski, *Polym. Adv. Technol.* **2002**, *13*, 615.
[40] a) W. Domagala, M. Laokowski, S. Guillerez, G. Bidan, *Electrochim. Acta* **2003**, *48*, 2379; b) K. Meerholz, J. Heinze, *Electrochim. Acta* **1996**, *41*, 1839.
[41] M.-H. Yoon, C. Kim, A. Facchetti, T. J. Marks, *J. Am. Chem. Soc.* **2006**, *128*, 12851.
[42] A. Abbotto, S. Bradamante, A. Facchetti, G. A. Pagani, *J. Org. Chem.* **2002**, *67*, 5753.
[43] a) J. Roncali, *Chem. Rev.* **1997**, *97*, 173; b) J. Casado, L. L. Miller, K. R. Mann, T. M. Pappenfus, V. Hernández, J. T. López Navarrete, *J. Phys. Chem. B* **2002**, *106*, 3597.
[44] a) J. Casado, R. Ponce Ortiz, M. C. Ruiz Delgado, V. Hernández, J. T. López Navarrete, J.-M. Raimundo, P. Blanchard, M. Allain, *J. Phys. Chem. B* **2005**, *109*, 16616; b) M. C. Ruiz Delgado, V. Hernán-

dez, J. Casado, J. T. López Navarrete, J. M. Raimundo, P. Blanchard, J. Roncali, *Chem. Eur. J.* **2003**, *9*, 3670.
[45] S. Hamai, F. Hirayama, *J. Phys. Chem.* **1983**, *87*, 83.
[46] B. Xu, S. Holdcroft, *Macromolecules* **1993**, *26*, 4457.
[47] M. Zander, *Z. Naturforsch. A: Phys. Sci.* **1989**, *44*, 1116.
[48] J. R. Larowicz, *Principles of fluorescence spectroscopy*; Kluwer Academic Press, New York, **1999**.
[49] M. Pope, C. E. Swenberg, *Electronic Processes in Organic Crystals*, Oxford University Press, New York, **1982**.
[50] a) J. Casado, V. Hernández, S. Hotta, J. T. López Navarrete, *Synth. Met.* **2001**, *119*, 305; b) C. Moreno Castro, M. C. Ruiz Delgado, V. Hernández, S. Hotta, J. Casado, J. T. López Navarrete, *J. Chem. Phys.* **2002**, *116*, 10419.
[51] A. Yassar, G. Horowitz, P. Valat, V. Wintgens, M. Hmyene, F. Deloffre, P. Srivastava, P. Lang, F. Garnier, *J. Phys. Chem.* **1995**, *99*, 9155.
[52] F. Garnier, *Acc. Chem. Res.* **1999**, *32*, 209.
[53] M. Muccini, E. Lunedei, C. Taliani, D. Beljonne, J. Cornil, J. L. Brédas, *J. Chem. Phys.* **1998**, *109*, 10513.
[54] H. Meng, J. Zheng, A. J. Lovinger, B.-C. Wang, P. G. Van Patten, Z. Bao, *Chem. Mater.* **2003**, *15*, 1778.
[55] a) V. Hernandez, J. Casado, F. J. Ramirez, G. Zotti, S. Hotta, J. T. Lopez Navarrete, *J. Chem. Phys.* **1996**, *104*, 9271; b) J. Casado, V. Hernandez, S. Hotta, J. T. Lopez Navarrete, *J. Chem. Phys.* **1998**, *109*, 10419; c) C. Moreno Castro, M. C. Ruiz Delgado, V. Hernandez, S. Hotta, J. Casado, J. T. Lopez Navarrete, *J. Chem. Phys.* **2002**, *116*, 10419; d) C. Moreno Castro, M. C. Ruiz Delgado, V. Hernandez, Y. Shirota, J. Casado, J. T. Lopez Navarrete, *J. Phys. Chem. B* **2002**, *106*, 7163.
[56] T. Kojima, J-I. Nishida, S. Tokito, H. Tada, Y. Yamashita, *Chem. Commun.* **2007**, 1430.
[57] a) T. Kojima, J-I. Nishida, S. Tokito, H. Tada, Y. Yamashita, *Chem. Commun.* **2007**, 1430; b) T. Yasuda, Y. Sakai, S. Aramaki, T. Yamamoto, *Chem. Mater.* **2005**, *17*, 6060; c) B. Ackers, A. J. Blake, S. J. Hill, P. Hubberstey, *Acta Crystallogr. Sect. C* **2002**, *58*, o640; d) F. Iwasaki, K.-Y. Akiba, *Acta Crystallogr. Sect. C* **1987**, *43*, 2338; e) R. Ghosh, S. H. Simonsen, *Acta Crystallogr. Sect. C* **1993**, *49*, 1031.
[58] a) J. Ma, S. Li, Y. Jiang, *Macromolecules* **2002**, *35*, 1109; b) M. Springborg, K. Schmidt, H. Meider, L. De Maria, *Organic Electronic Materials: Conjugated Polymers and Low Molecular Weight Organic Solids, Vol. 41* (Ed.: G. Grosso), Springer, Berlin, **2001**, p. 39; c) J.-L. Brédas, J. Cornil, D. Beljonne, D. A. Dos Santos, Z. Shuai, *Acc. Chem. Res.* **1999**, *32*, 267; d) S. Stafström, J.-L. Bredas, *Theochem* **1989**, *183–203*, 393; e) G. R. Hutchison, M. A. Ratner, T. J. Marks, *J. Phys. Chem. A* **2002**, *106*, 10596.
[59] W. J. Hehre, *A Guide to Molecular Mechanics and Quantum Chemical Calculations*, Wavefunction, Irvine, **2003**.
[60] a) F. Grein, *THEOCHEM* **2003**, *624*, 23; b) A. A. Mohamed, *Int. J. Quantum Chem.* **2000**, *79*, 367; c) F. Grein, *J. Phys. Chem. A* **2002**, *106*, 3823.
[61] a) O. V. Prezhdo, *Adv. Mater.* **2002**, *14*, 597; b) J. Wang, B. G. Johnson, R. J. Boyd, L. A. Eriksson, *J. Phys. Chem.* **1996**, *100*, 6317.
[62] J. C. Rienstra-Kiracofe, G. S. Tschumper, H. F. Schaefer, S. Nandi, G. B. Ellison, *Chem. Rev.* **2002**, *102*, 231.
[63] C. G. Zhan, J. A. Nichols, D. A. Dixon, *J. Phys. Chem. A* **2003**, *107*, 4184.
[64] C. G. Zhan, J. A. Nichols, D. A. Dixon, *J. Phys. Chem. A* **2003**, *107*, 4184.
[65] J. Muscat, A. Wander, N. M. Harrison, *Chem. Phys. Lett.* **2001**, *342*, 397.
[66] G. R. Hutchison, A. Facchetti, M. A. Ratner, T. J. Marks, unpublished results.
[67] a) D. Fichou, *J. Mater. Chem.* **2000**, *10*, 571; b) T. Siegrist, C. Kloc, R. A. Laudise, H. E. Katz, R. C. Haddon, *Adv. Mater.* **1998**, *10*, 379; c) L. Antolini, G. Horowitz, F. Kouki, F. Garnier, *Adv. Mater.* **1998**, *10*, 382.
[68] **α6**: a) G. J. Visser, G. J. Heeres, J. Wolters, A. Vos, *Acta Crystallogr., Sect. B* **1968**, *24*, 467; b) M. Pelletier, F. Brisse, *Acta Crystallogr. Sect. A* **1994**, *50*, 1942; **α5**: c) L. Antolini, G. Horowitz, F. Kouki, F. Garnier, *Adv. Mater.* **1998**, *10*, 382; d) T. Siegrist, C. Kloc, R. A. Laudise, H. E. Katz, R. C. Haddon, *Adv. Mater.* **1998**, *10*, 379; **α4**: e) G. Horowitz, B. Bachet, A. Yassar, P. Lang, F. Demanze, J.-L. Fave, F. Garnier, *Chem. Mater.* **1995**, *7*, 1337.
[69] *Handbook of Chemistry and Physics*, CRC Press, Boca Raton, **1995**.
[70] The energy level of the normal hydrogen electrode (NHE) is −4.6 eV below the vacuum level (see A. J. Bard, L. R. Faulkner, *Electrochemical Methods —Fundamentals and Applications*, Wiley, New York, **1984**). The oxidation potential of ferrocene is 0.67 V versus the NHE (see J.-F. Wang, Y. Kawabe, S. E. Shaheen, M. M. Morrell, G. E. Jabbour, P. A. Lee, J. Anderson, N. R. Armstrong, B. Kippelen, E. A. Mash, N. Peyghambarian, *Adv. Mater.* **1998**, *10*, 230). The HOMO/LUMO energies were determined using the ferrocene calibration against the vacuum energy level. The terms HOMO and LUMO are a convenient short hand since the actual energies correspond to states, not levels.
[71] a) R. W. Godby, M. Schluter, L. J. Sham, *Phys. Rev. B* **1988**, *37*, 10159; b) R. Stowasser, R. Hoffmann, *J. Am. Chem. Soc.* **1999**, *121*, 3414.
[72] M. J. Kamlet, J. L. M. Abboud, M. H. Abraham, R. W. Taft, *J. Org. Chem.* **1983**, *48*, 2877.
[73] M. Jonsson, A. Houmam, G. Jocys, D. D. M. Wayner, *J. Chem. Soc. Perkin Trans. 2* **1999**, 425.
[74] V. Hernández, J. T. López Navarrete, *J. Chem. Phys.* **1994**, *101*, 1369.
[75] a) R. S. Becker, J. Seixas de Melo, A. L. Macanita, F. Elisei, *Pure Appl. Chem.* **1995**, *67*, 9; b) R. S. Becker, J. Seixas de Melo, A. L. Macanita, F. Elisei, *J. Phys. Chem.* **1996**, *100*, 18683; c) D. Beljonne, J. Cornil, R. H. Friend, R. A. J. Janssen, J. L. Brédas, *J. Am. Chem. Soc.* **1996**, *118*, 6453; d) J. Seixas de Melo, L. M. Silva, L. G. Arnaut, R. S. Becker, *J. Chem. Phys.* **1999**, *111*, 5427.
[76] K. Schmidt, S. Brovelli, V. Coropceanu, D. Beljonne, J. Cornil, C. Bazzini, T. Caronna, R. Tubino, F. Meinardi, Z. Shuai, J. L. Brédas, *J. Phys. Chem. A* **2007**, *111*, 10490.
[77] A. Facchetti, M. Mushrush, M.-H. Yoon, G. R. Hutchison, M. A. Ratner, T. J. Marks, *J. Am. Chem. Soc.* **2004**, *126*, 13874.
[78] M. Malagoli, J. L. Bredas, *Chem. Phys. Lett.* **2000**, *327*, 13.
[79] Y. Wei, Y. Yang, J.-M. Yeh, *Chem. Mater.* **1996**, *8*, 2659.
[80] A. Facchetti, M.-H. Yoon, C. L. Stern, G. R. Hutchison, M. A. Ratner, T. J. Marks, *J. Am. Chem. Soc.* **2004**, *126*, 13480.
[81] S. Dufresne, G. S. Hanan, W. G. Skene, *J. Phys. Chem. B* **2007**, *111*, 11407.
[82] a) A. J. Goodman, S. P. Stanforth, B. Tarbit, *Tetrahedron* **1999**, *55*, 15067.
[83] Gaussian 03, Revision B.04, M. J. Frisch, G. W. Trucks, H. B. Schlegel, G. E. Scuseria, M. A. Robb, J. R. Cheeseman, J. A. Montgomery, Jr., T. Vreven, K. N. Kudin, J. C. Burant, J. M. Millam, S. S. Iyengar, J. Tomasi, V. Barone, B. Mennucci, M. Cossi, G. Scalmani, N. Rega, G. A. Petersson, H. Nakatsuji, M. Hada, M. Ehara, K. Toyota, R. Fukuda, J. Hasegawa, M. Ishida, T. Nakajima, Y. Honda, O. Kitao, H. Nakai, M. Klene, X. Li, J. E. Knox, H. P. Hratchian, J. B. Cross, V. Bakken, C. Adamo, J. Jaramillo, R. Gomperts, R. E. Stratmann, O. Yazyev, A. J. Austin, R. Cammi, C. Pomelli, J. W. Ochterski, P. Y. Ayala, K. Morokuma, G. A. Voth, P. Salvador, J. J. Dannenberg, V. G. Zakrzewski, S. Dapprich, A. D. Daniels, M. C. Strain, O. Farkas, D. K. Malick, A. D. Rabuck, K. Raghavachari, J. B. Foresman, J. V. Ortiz, Q. Cui, A. G. Baboul, S. Clifford, J. Cioslowski, B. B. Stefanov, G. Liu, A. Liashenko, P. Piskorz, I. Komaromi, R. L. Martin, D. J. Fox, T. Keith, M. A. Al-Laham, C. Y. Peng, A. Nanayakkara, M. Challacombe, P. M. W. Gill, B. Johnson, W. Chen, M. W. Wong, C. Gonzalez, J. A. Pople, Gaussian, Inc., Pittsburgh PA, **2003**
[84] A. D. Becke, *J. Chem. Phys.* **1993**, *98*, 1372.
[85] a) P. J. Stephens, F. J. Devlin, F. C. F. Chabalowski, M. J. Frisch, *J. Phys. Chem.* **1994**, *98*, 11623; b) J. J. Novoa, C. Sosa, *J. Phys. Chem.* **1995**, *99*, 15837.
[86] a) A. P. Scott, L. Radom, *J. Phys. Chem.* **1996**, *100*, 16502; b) G. Rauhut, P. Pulay, *J. Phys. Chem.* **1995**, *99*, 3093.
[87] M. M. Francl, W. J. Pietro, W. J. Hehre, J. S. Binkley, M. S. Gordon, D. J. Defrees, J. A. Pople, *J. Chem. Phys.* **1982**, *77*, 3654.

[88] a) E. Runge, E. K. U. Gross, *Phys. Rev. Lett.* **1984**, *52*, 997; b) E. K. U. Gross, W. Kohn, *Adv .Quantum Chem.* **1990**, *21*, 255; c) Density Functional Theory (Eds.: E. K. U. Gross, R. M. Driezler), Plenum Press, New York, **1995**, p. 149; d) M. E. Casida, *Recent Advances in Density Functional Methods, Part I* (Ed.: D. P. Chong), World Scientific, Singapore, **1995**, p. 115.

[89] J. B. Foresman, M. Head-Gordon, J. A. Pople, M. J. Frish, *J. Phys. Chem.* **1992**, *96*, 135.

Received: November 20, 2008
Published online: February 27, 2009

